N72-23153

CASE FILE
COPY

TM-(L)-HU-033/005/00

ANALYSES OF REQUIREMENTS FOR COMPUTER CONTROL AND DATA PROCESSING EXPERIMENT SUBSYSTEMS

ATM EXPERIMENT S-056

IMAGE DATA PROCESSING SYSTEM

TECHNIQUE DEVELOPMENT

VOLUME I

15 MARCH 1972

SYSTEM DEVELOPMENT CORPORATION • 2500 COLORADO AVENUE • SANTA MONICA, CALIFORNIA 90406

SERIES BASE NO. / VOL. / REISSUE

TM-(L)-HU-033/005/00

TECHNICAL MEMORANDUM

(TM Series)

This document was produced by SDC in performance of contract NAS8-25471

ATM EXPERIMENT

S-056

IMAGE DATA PROCESSING SYSTEM

TECHNIQUE DEVELOPMENT

VOLUME I

15 MARCH 1972

SYSTEM DEVELOPMENT CORPORATION

4810 BRADFORD BLVD., N. W.

HUNTSVILLE

ALABAMA

35805

TABLE OF CONTENTS

	Page No.
FORWARD	v
1. INTRODUCTION	1-1
1.1 EXPERIMENT DESIGN	1-2
1.1.1 The Telescope Optical System	1-2
1.1.2 S-056 Flight Film Characteristics	1-4
1.2 EXPERIMENT TEST PROGRAM	1-5
1.3 PROJECT WORK BASIS	1-10
1.3.1 Picture Blur	1-10
1.3.2 Noise	1-16
1.3.3 Nonlinearity	1-16
2. TECHNICAL APPROACH	2-1
2.1 PHASE A ACTIVITIES	2-1
2.1.1 Compatibility Guidelines	2-3
2.1.2 Utility Software	2-4
2.1.3 Noise Removal	2-5
2.2 PHASE B ACTIVITIES	2-5
2.2.1 Deconvolution	2-6
2.2.2 Technique Evaluation	2-6
3. TECHNIQUE DEVELOPMENT	3-1
3.1 PRINCIPLES OF DECONVOLUTION	3-2
3.2 CONDITIONS FOR SUCCESSFUL DECONVOLUTION	3-4
3.2.1 Image Conversion Accuracy	3-4
3.2.1.1 Sampling Resolution	3-5
3.2.1.2 Quantizing Resolution	3-5
3.2.2 Film Data Linearity	3-9
3.2.2.1 Linearization	3-12
3.2.2.2 Enhancement	3-12
3.2.3 Noise	3-15
3.2.3.1 Random Noise	3-15
3.2.3.2 Correlated Noise	3-20

TABLE OF CONTENTS (continued)

Page No.

3.2.4 System PSF. 3-21
3.3 APPLICATION TO REAL DATA 3-28
3.3.1 PSF Estimation. 3-29
3.3.2 Deconvolution Controls. 3-32
3.3.2.1 Scaling. 3-32
3.3.2.2 Frequency Selection Processing 3-35
3.3.2.3 Amplification Limiting 3-36

4. CONCLUSIONS AND RECOMMENDATIONS. 4-1
4.1 CONCLUSIONS. 4-1
4.2 RECOMMENDATIONS. 4-2

REFERENCES. R-1

BIBLIOGRAPHY. B-1

APPENDIX A. A-1

LIST OF FIGURES

Figure 1 Principle Employed by Glancing Incidence X-ray Optics. . . . 1-2
Figure 2 Glancing Incidence Solar Telescope Showing Integration of X-ray Optics with Film Transport. 1-3
Figure 3 Basic S-056 Film Construction. 1-4
Figure 4 Equipment Setup for Making Telescope Test Using Collimated Test Pattern. 1-5
Figure 5 Test Target Used in Testing the S-056 Telescope in Face-To-Face Configuration 1-6
Figure 6 Photomicrograph of Resolution Chart Photographed in Visible Light on a High Resolution Glass Plate in the Face-To-Face Configuration 1-7

LIST OF FIGURES (continued)

		Page No.
Figure 7	Photomicrograph of Resolution Chart Photographed in Visible Light in Face-To-Face Test Configuration on Flight Film.	1-8
Figure 8	Photomicrograph of X-ray (8Å) Illuminated Test Target Photographed in the Face-To-Face Test Configuration on Flight Film.	1-9
Figure 9	Example Resolution Chart	1-10
Figure 10	Two-Dimensional Plot Along Dashed Line of Figure 9	1-11
Figure 11	Illustrative Example of Picture Sampling	1-12
Figure 12	Illustration of the Results of the Sampling in Figure 11	1-13
Figure 13	Point Spread Function Profiles	1-14
Figure 14	Summation of PSF Curves to Illustrate Convolution.	1-15
Figure 15	Work Plan and Performance Schedule	2-2
Figure 16	Image Restoration Project Work Situation	3-1
Figure 17	S-056 Image System Degradation	3-2
Figure 18	Study of the Effects of Quantization on the Deconvolution Process.	3-6
Figure 19	Study of the Effects of Quantization and Extent of Blur on the Deconvolution Process	3-7
Figure 20	Application of Frequency Term Application Limiting to Deconvolution of Image With Varying Levels of Blur and Quantization Rate.	3-9
Figure 21	Characteristic D Log_{10} E Film Curve.	3-11
Figure 22	Illustration of Image Enhancement.	3-13
Figure 23	Enhancement of a Fogged Image.	3-14
Figure 24	Study of the Effectiveness of Multiple-Frame Averaging for Noise Reduction Prior to Deconvolution	3-17
Figure 25	Display of the Logarithm of Fourier Transform Magnitude Terms.	3-18
Figure 26	Illustration of the Use of Band Reject Filtering for the Removal of Correlated Noise.	3-21
Figure 27	Theoretical Prediction of S-056 PSF for On-Axis Images at Infinity.	3-23

LIST OF FIGURES (continued)

		Page No.
Figure 28	Computer Generated Resolution Chart Used in Testing the Dependency of Deconvolution on Accurate PSF Determination.	3-25
Figure 29	Computer Generated Resolution Chart Blurred by Convolution With Predicted S-056 PSF	3-25
Figure 30	3 x 3 Array of Variations on Predicted S-056 PSF	3-26
Figure 31	Results of the Deconvolution of the Blurred Image in Figure 29 With Each of the PSF's in Figure 30.	3-27
Figure 32	Visible Light Frame 9 After Scanning With a Microdensitometer and Re-recording on Film	3-29
Figure 33	Results of the Deconvolution of Visible Light Frame 9 With an Array of Trial PSF's.	3-30
Figure 34	Comparison of PSF Producing Best Deconvolution of Visible Light Frame 9.	3-31
Figure 35	Results of Scaling the Data from the Deconvolution of Visible Light Frame 9 Between the High/Low Limits in Figure 36.	3-34
Figure 36	Image Clipping Levels.	3-34
Figure 37	Result of Frequency Selection Processing of Center Picture in Figure 35	3-36
Figure 38	Deconvolved Resolution Chart With Overamplification of Certain Frequency Terms.	3-37
Figure 39	Results of Repeating the Deconvolution Illustrated in Figure 38 With Term Amplification Limited to: (a) 100,000 (b) 30,000; (c) 1,000.	3-38

FORWARD

This document is the first of two produced under NASA contract number NAS8-25471, "Analyses of Requirements for Computer Control and Data Processing Experiment Subsystems." This report was prepared by the Huntsville Space Projects staff of System Development Corporation for the Computer Systems Division of the George C. Marshall Space Flight Center's Computation Laboratory. Volume I, ATM Experiment S-056, Image Data Processing System/Technique Development, presents the results of the image processing studies for S-056 pictures and Volume II, ATM Experiment S-056, Image Data Processing System/Software Development, documents the software designed and implemented by SDC in support of the image processing studies.

This work was performed under the technical direction of Mr. Bobby C. Hodges, Contracting Officer's Representative for the project. Appreciation is expressed to Mr. Hodges, Mr. Doug Thomas and Dr. E. H. Hopper of the MSFC Computation Laboratory and to Mr. J. E. Milligan of Space Sciences Laboratory for their support and technical assistance during the course of this project.

SECTION 1. INTRODUCTION

During the past decade, most photographs from space have been transmitted to the earth in electronic form. As a result, image resolution has been limited, and high noise levels have been experienced. The return of more than a thousand frames of large format, high resolution photographs of the lunar surface by the Apollo 15 Spacecraft marked the beginning of a new phase of space exploration. In the future, such missions as planned for the NASA Skylab program will return scientific image data to earth in its original photographic format -- limited only by the imaging characteristics of the scientific instrument used, the film on which the data is recorded, and the prevailing seeing conditions in space. To support these experiments, new techniques are needed for processing image data which take advantage of the superior storage and retrieval characteristic of photographic film.

The Solar Imaging X-ray Telescope Experiment (designated the S-056 experiment) is typical of several of the astronomy experiments of the Skylab programs. It will photograph the sun in the far ultra-violet or soft X-ray region and will produce a total of some 24,000 photographs. Because of the imaging characteristics of this telescope and the necessity of using special techniques for capturing images on film at these wave lengths, it became evident that improved methods for computer processing of the S-056 photographs was needed. Consequently, the System Development Corporation was given the task of developing techniques for processing image data from the S-056 experiment. Specifically, the problems of image restoration were to be addressed to develop and test digital computer techniques for applying a deconvolution process to restore overall S-056 image quality. Additional techniques for reducing or eliminating the effects of noise and nonlinearity in S-056 photographs would be developed in support of the deconvolution effort.

This report presents the results of the above effort. It is contained in two volumes -- Volume I (Technique Development) presents the approach, findings, and conclusions of the project, and Volume II (Software Development) documents the software produced.

1.1 EXPERIMENT DESIGN

A general understanding of two design features is pertinent to the development of image processing techniques for the S-056 experiment:

- The telescope optical system
- S-056 flight film characteristics

1.1.1 The Telescope Optical System

The X-ray imaging solar telescope makes use of a discovery made by A. H. Compton in 1923. He found that X-rays can be reflected from polished surfaces if they strike the surface of a small angle of incidence. This principle can be employed as shown in Figure 1 by constructing a surface of revolution in the form of a truncated paraboloid/hyperboloid and locating a film carrier at the focus.

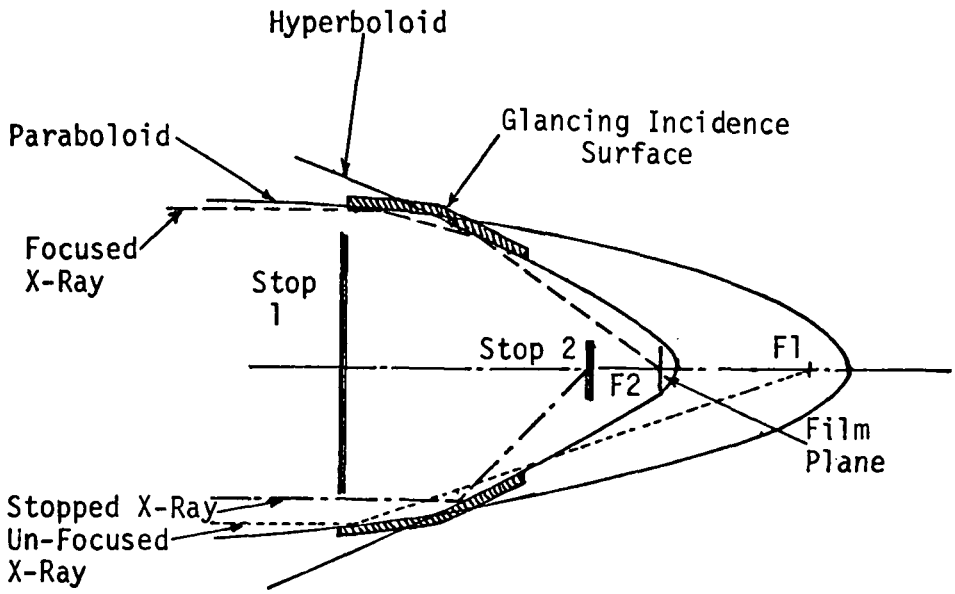


Figure 1 - Principle Employed by Glancing Incidence X-ray Optics. (The angles of incidence have been exaggerated for clarity.)

Parallel rays from a distant object are reflected from each surface in turn and are focused at F2 to form a real, inverted image. Opaque disks act as optical masks or stops to intercept X-rays which would not strike both optical surfaces and consequently would not be focused by the telescope.

Figure 2 illustrates how a film camera will be integrated into the S-056 glancing incidence telescope. In addition to the normal film advance and shutter mechanisms, a set of six camera filters are used to record X-ray filter-grams. The X-ray filters provide a spectral resolution of 2-1/2 angstroms (Å) over a two-band range of 5-20Å and 27-33Å. The telescope itself exhibits a spatial resolution capability of 2.5 sec of arc with a field of view of 40 min of arc. Camera shutter, film advance, and filter wheel operation are controllable through an experiment electronics package from an experiment control panel within the Skylab.

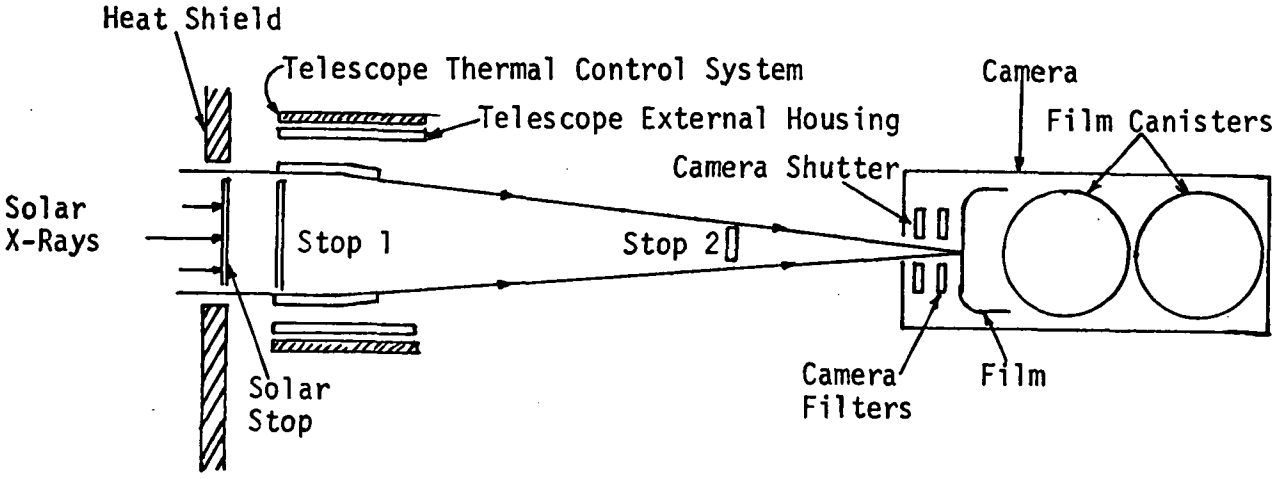


Figure 2 - Glancing Incidence Solar Telescope Showing Integration of X-ray Optics with Film Transport

The S-056 glancing incidence telescope is mounted as an integral part of the Apollo Telescope Mount (ATM) assembly which is kept pointed at the sun by an automatic pointing control system. During periods of low interest, the S-056 camera is operated in automatic "Patrol" mode by timers within the experiment electronics package. In this mode, pictures are made through each of the six spectral filters at a slow rate for as long as the experiment is in that mode. By going to a manual "Single Frame" mode, single pictures can be made through any one of the six filters. During periods of high interest, a semi-automatic "Active" mode is used for taking multiple frame sequences of photographs. Each sequence consists of one exposure at each of a number of filter positions made in sequence. Exposure times of each frame can be selected for long, normal, or short duration.

When the film in a film canister is depleted or at the end of the mission, an astronaut will retrieve the exposed film and replace it with a fresh canister. Exposed film is returned to earth by the Apollo Spacecraft and turned over to the experiment Principal Investigator.

1.1.2 S-056 Flight Film Characteristics

The S-056 telescope operates in a band of the electromagnetic spectrum where radiation is easily absorbed by any dense material through which it passes. Such radiation is even absorbed by the thin gelatin coating of most photographic films. For this reason, a special film was designed which has no such gelatin overcoat so that the soft X-radiation can expose the film emulsion granules. Figure 3 illustrates how the S-056 film is constructed.

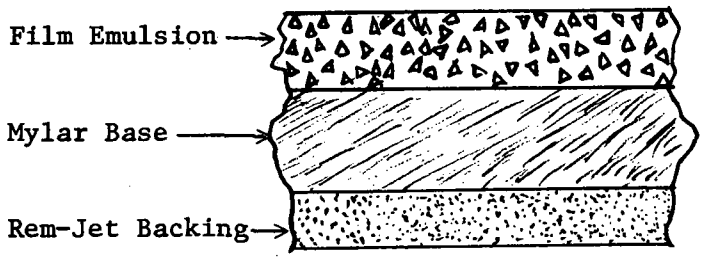


Figure 3 - Basic S-056 Film Construction

The silver halide film grains are imbedded in a gelatin binder with little or no gelatin between the outermost grains and the film surface. Because of the absorption characteristic of the binder, only the film grains nearest the surface will be exposed by the soft X-radiation. The film base is thin (2.5 mil) Mylar. A special backing called Rem-Jet is used with the S-056 film. The Rem-Jet backing balances the film to prevent curling and reduces the possibility of film exposure through friction induced static discharge.

1.2 EXPERIMENT TEST PROGRAM

Throughout its entire development, S-056 components, subassemblies, and major assemblies have been extensively tested. One particular series of tests is especially relevant to this report -- the tests of telescope imaging characteristics using a collimated test pattern.

In order to test the ability of the S-056 telescope to resolve an image at infinity, a test image must either be located at a great distance from the telescope, or the light from the test image must be collimated to produce rays which are parallel. Both methods have been used to test the S-056 telescope, but the latter method is most relevant to this report because photographs of collimated test targets were used for image processing technique development during the past year. Figure 4 illustrates a setup used for making X-ray tests of the S-056 telescope.

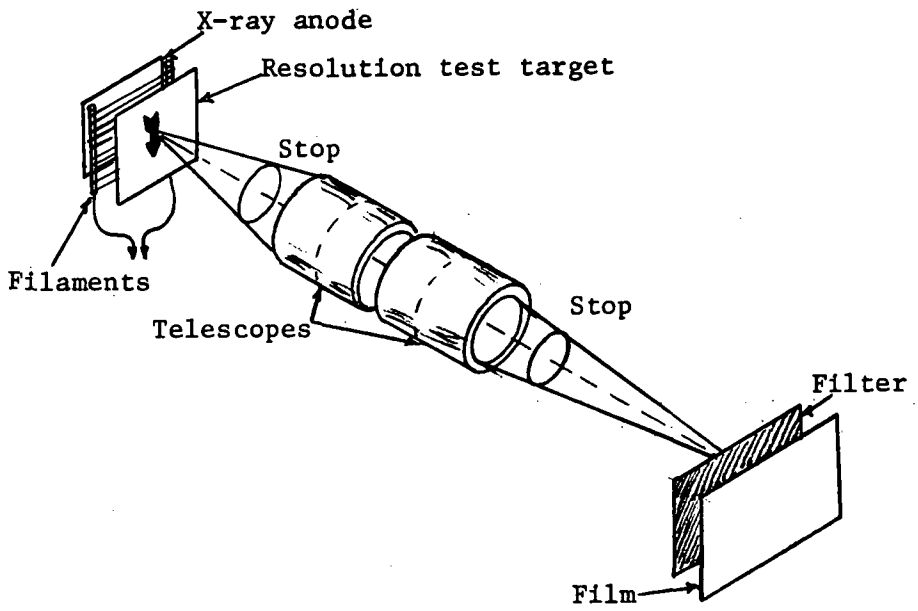


Figure 4 - Equipment Setup for Making Telescope Tests Using Collimated Test Patterns

For these tests, two identical telescopes were used -- one to collimate the light from the test image, and one to focus the image on photographic film. The two telescopes were mounted face-to-face on a rigid optical bench and very accurately aligned along a common longitudinal axis. A special test image generator was

constructed to generate a reasonably uniform source of soft X-rays since such devices are not commonly available. The test image itself was a modified Air Force resolution target. Figure 5 is a print of the modified target. The original was a template -- chemically etched in a sheet of copper. The original modified target has an edge-to-edge dimension of approximately one millimeter.

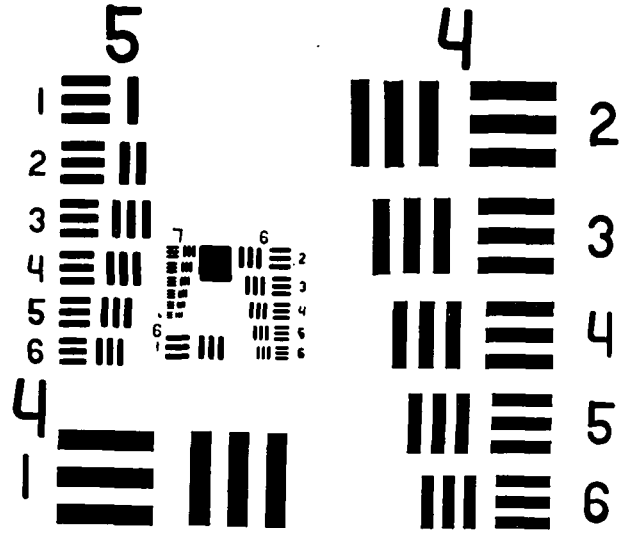


Figure 5 - Test Target Used in Testing the S-056 Telescope in Face-To-Face Configuration

When photographed by the S-056 telescope in the face-to-face configuration of Figure 4 this test setup produces bars in the largest group (4-1) which represents approximately 9 sec of arc /line pair and bars in the smallest group (7-6) of approximately 0.6 sec of arc/line pair.

In order to eliminate the noise and resolution limitations of the flight film, tests were made using extremely fine grain glass plates in place of the flight film. This effectively isolated telescope losses to those of the glancing incidence optics so that subsequent evaluation could be made of the losses caused by the flight film. Figure 6 is a photomicrograph of one of the glass plate test pictures.

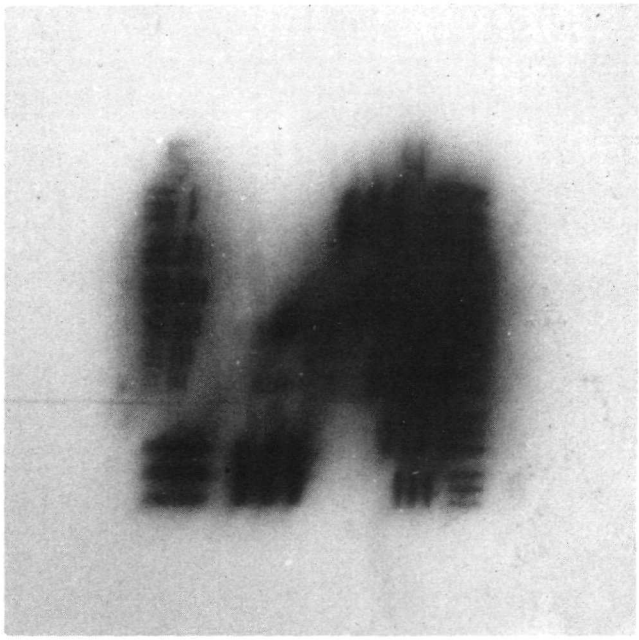


Figure 6 - Photomicrograph of Resolution Chart Photographed in Visible Light on a High Resolution Glass Plate in the Face-to-Face Configuration

Resolution bars down to group (6-1) are recorded indicating a resolution limit of 2.3 sec of arc in telescope optics when using high resolution glass plates. Photographs were made on flight film using both soft X-ray and visible light illumination. Figure 7 is a photomicrograph of a picture made by the S-056 telescope in the face-to-face test configuration using visible light illumination.

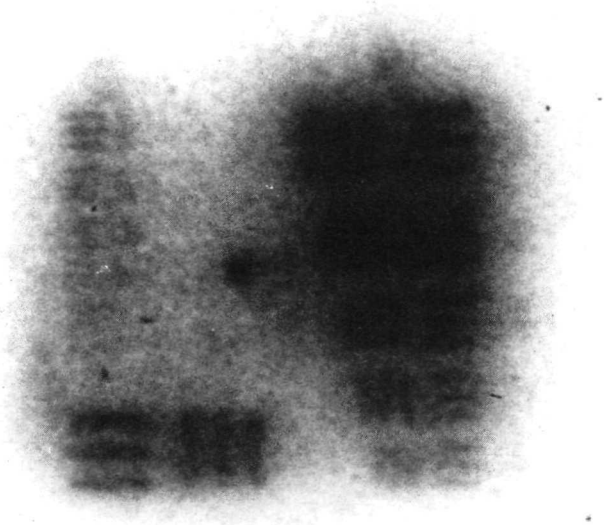


Figure 7 - Photomicrograph of Resolution Chart Photographed in Visible Light in Face-To-Face Test Configuration on Flight Film

Resolution bars down to group (5-1) are evident indicating a telescope resolution limit of 4 sec of arc using flight film.

Figure 8 is a photomicrograph of the test target made by the S-056 telescope in the face-to-face test configuration using X-ray illumination (8Å).

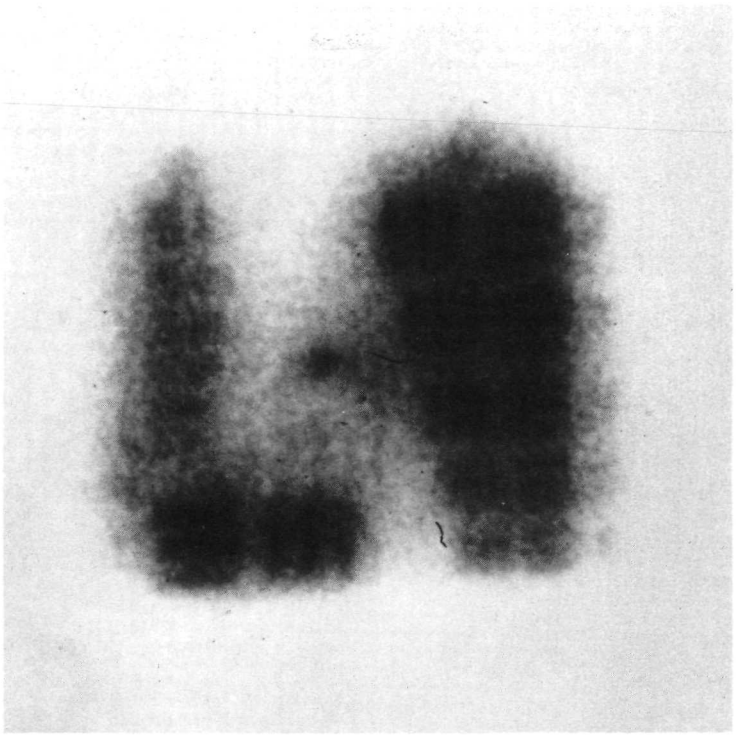


Figure 8 - Photomicrograph of X-ray (8Å) Illuminated Test Target Photographed in the Face-To-Face Test Configuration on Flight Film

Resolution bars down to group (4-6) are visible indicating a resolution limit of 4.5 sec of arc. An increased level of noise is apparent in the flight film as a result of the difference in film latitudes of the glass plates and flight film. Random scattering is much more severe in the X-ray photos indicating a greater sensitivity to surface irregularities at the X-ray wave lengths.

Since the blurring effects of two telescopes are manifest in Figures 6, 7, and 8, the resolution of a single telescope in space could reasonably be expected to double. That is, the S-056 telescope in space could be expected to resolve images down to 2.5 sec of arc on flight film.

1.3 PROJECT WORK BASIS

Since image blur or scattering represents the greatest factor in limiting S-056 telescope resolution, it is natural that the reduction of blur would receive first attention in preparing for the future processing of S-056 flight film data. In order to discuss the elements of the reduction of blur, it is first necessary to understand the factors contributing to blur and how the physical phenomenon of blur may be described mathematically. An understanding of the origins of film noise and non-linearity is also important since these two factors greatly influence the success of any attempts to reduce blur.

1.3.1 Picture Blur

An understanding of the phenomenon of picture blur is best obtained by employing the common analytic approach of breaking a function (in this case -- the picture) down into very small elements (in this case -- spots of light). If a visual scene is broken down into a two dimensional array of spots of light of varying intensity, an understanding of what happens when the scene is blurred by an optical system can be obtained by an examination of the changes which take place in the elemental spots of light. The problem is simplified by working initially in a single dimension. Consider first the simple resolution chart in Figure 9.

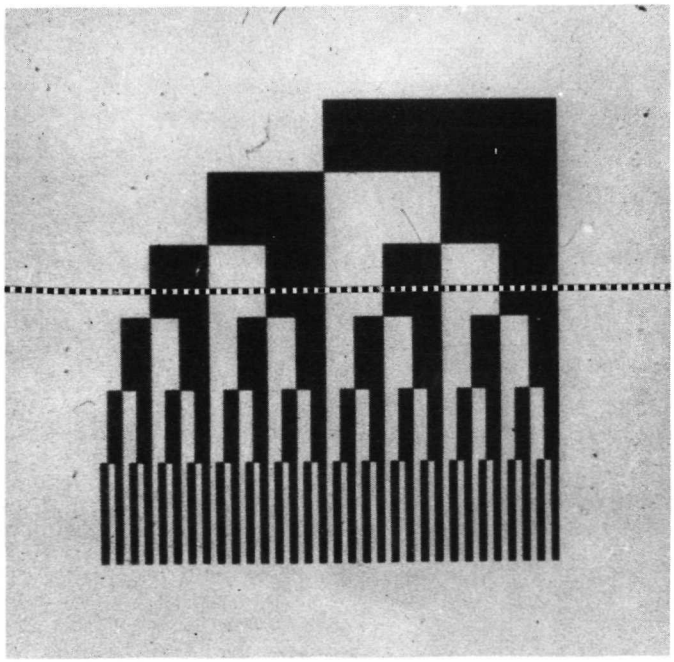


Figure 9 - Example Resolution Chart

If the chart is examined along the single dimension indicated by the dashed line, and if a plot is made of the degree of blackness with respect to the position along the dashed line (assigning an arbitrary value of 1.0 for completely black and 0. for completely white areas) the graph shown in Figure 10 will result.

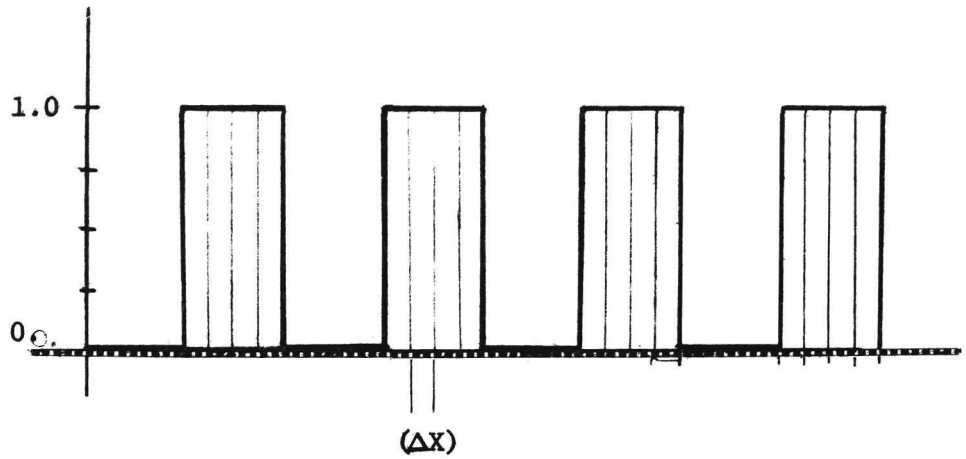


Figure 10 - Two Dimensional Plot Along Dashed Line of Figure 9

By breaking the plot in Figure 10 down further into a large number of increments (ΔX), and assigning a number between 0. - 1.0 corresponding to the degree of blackness or "level of gray" to each increment, the line across the picture can be reduced to a table of numbers. A picture may be described by applying a similar procedure to produce a two dimensional array of incremental values (ΔX, ΔY). Figure 11 illustrates how a familiar portrait may be segmented in this manner. This process of breaking a picture down into a two dimensional array of values will be referred to as picture "sampling", and the process of describing the sampled picture values by a numeric relationship will be referred to as "quantization".

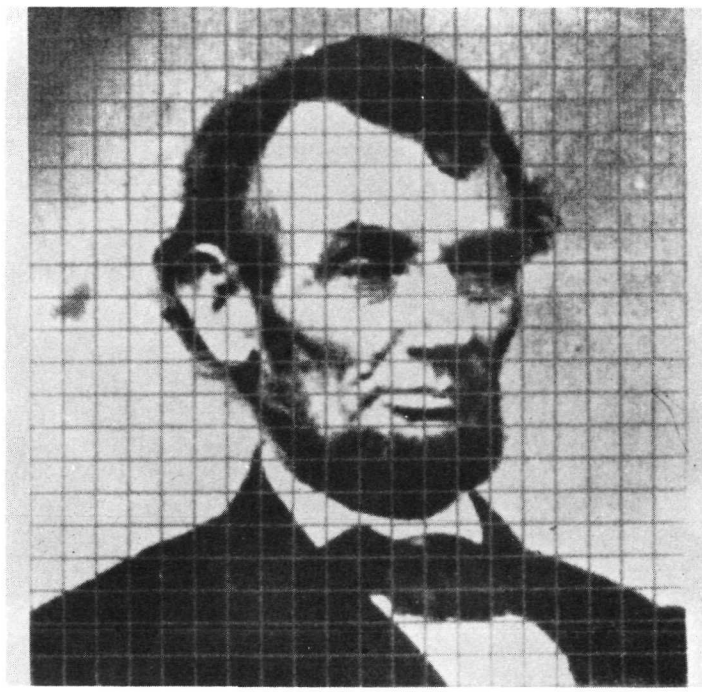


Figure 11 - Illustrative Example of Picture Sampling

The accuracy with which a picture may be described through sampling and quantization depends upon the number of picture values used for sampling and the number of "gray levels" used in the quantization. Figure 12 illustrates the result of sampling the portrait in Figure 11 with a small number of sampling values (484).

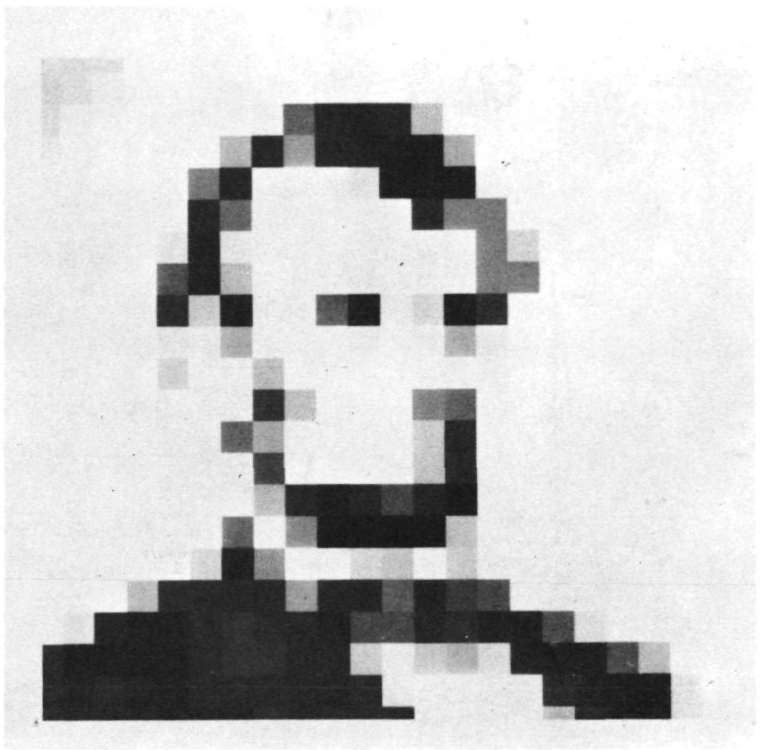


Figure 12 - Illustration of the Results of the Sampling in Figure 11

If a visual scene is sampled with a very large number of points (for example, a 1000 x 1000 array) a single sample value may be thought of as a unit impulse whose amplitude corresponds to the level of light intensity (see Figure 13-a).

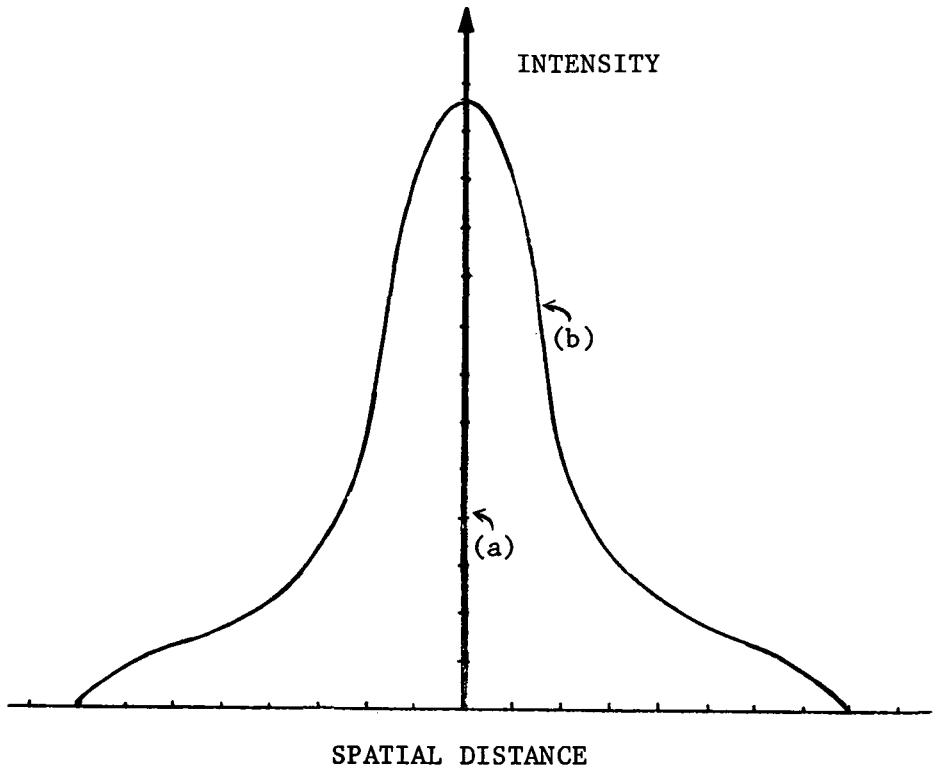


Figure 13 - Point Spread Function Profiles
(a) Ideal; (b) Real

If this unit impulse (or spot of light) is photographed with an optical system which blurs the image, the profiles of the single spot will be changed and will occupy a larger area than it did in the original array (see Figure 13(b)). The function which results from the passage of a unit light impulse through an optical system is called the point spread function (PSF) of the system and is an accurate descriptor of the blurring characteristics of the optical system.

Although a point spread function is generally a three-dimensional function, its effect in modifying an input image is easier visualized in two dimensions. Consider again the plot of picture values in Figure 10. If each of the ΔX picture values is considered as a unit light impulse value, each impulse will be modified accourding to a curve similar to Figure 13(b) (see Figure 14(a)).

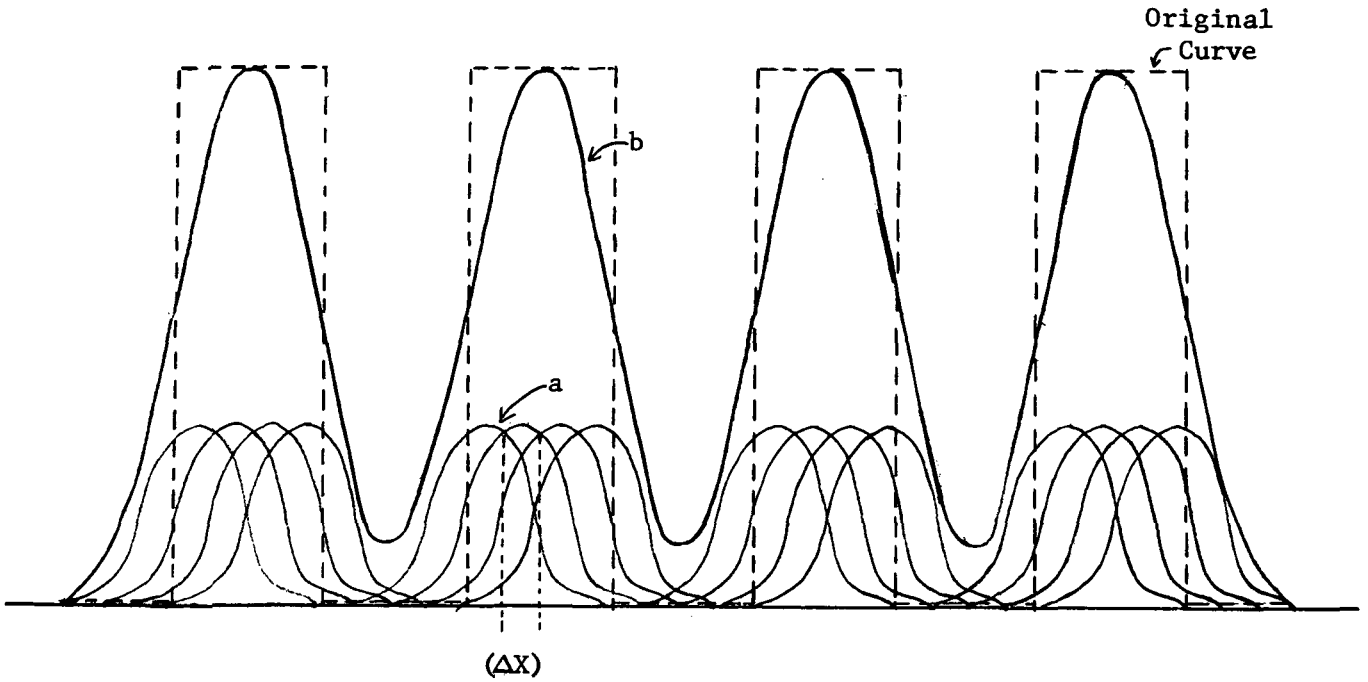


Figure 14 - Summation of PSF Curves To Illustrate Convolution (a - Component PSF's; b - Summation Curve)

Since the resulting curves now overlap into the area of their neighbors, the resulting picture will be the summation or average of all the curves taken together (see Figure 14-b). This process of modification of an input picture function with a point spread function is a simple illustration of the mathematical process called "convolution". For purposes of introduction, the assumption is made that the distortion is uniform over the field of view. When performed in two dimensions the mathematical convolution of a light intensity array with a point spread function accurately describes image blur. Since it is therefore possible to describe blur mathematically, it is theoretically possible to reverse the process and "de-blur" a picture. This process of reverse convolution or "de-blurring" is called "deconvolution". It is the theoretical basis for a major portion of the image restoration work of the past year.

1.3.2 Noise

The success with which the deconvolution process may be applied to "de-blur" a picture depends heavily on the amount of noise present in the original photograph. The term "noise" may apply to a number of characteristics of a picture but for the purposes of this report picture noise may be thought of as any variation of image data from the predictable result of recording a focused image on an idealized recording medium (a nonlinear film recording characteristic is assumed). In other words, if the difference between the photographic data and the original image can't be described by the convolution of the image with a predictable point spread function, taking into account a known film recording non-linearity, then those differences are described as noise.

Noise occurs in two forms -- random noise and periodic noise. Random noise results from such influences as film granularity and stray radiation and is the most difficult to eliminate. Periodic or correlated noise is more easily eliminated from photographic data because of its predictability. The isolation and removal or reduction of these two forms of noise is vital to the future processing of S-056 image data and has formed the basis for a significant portion of the project effort.

1.3.3 Nonlinearity

Under ideal conditions S-056 image data would be recorded on a photographic film which yields film density variations as a direct linear function of the X-ray intensity. Unfortunately, this will not be the case and a nonlinear density/intensity relationship must be assumed. Since the blurring which takes place in the S-056 optics is the physical convolution of light intensities with a point spread function, it is important that the data operated on by the deconvolution process be expressed as intensity and not film density. For this reason, each sampled picture value in the picture array should be corrected by applying a non-linear correction curve before deconvolution is attempted. Development of the techniques for correcting for nonlinear film response has been the basis for another significant portion of the project effort.

SECTION 2. TECHNICAL APPROACH

The System Development Corporation's effort to develop techniques for processing image data from the S-056 experiment began on March 15, 1971. At that time no image processing hardware was available and, with the exception of the IBM 7094 computer, very little was known about the characteristics of the equipment which would be provided. An IBM 7094 Mod I computer was installed in April but it was not until August, when photo scanning and recording equipment was delivered, that work with real photographs was possible. During the period from April to August, efforts were focused on developing general techniques for handling image data and for establishing guidelines for the development of hardware dependent computer routines. Because there was no computer software available at MSFC for image processing, a portion of the first four months of contract activity was spent in designing a software operating system for image processing.

The technical approach of the project was broken into two work phases. Phase A activities established guidelines for developing software needed to handle image data formats, developed general utility routines for input, output, reformating, and control of image data, and investigated preliminary methods for removing or reducing noise in image data. Phase B activities addressed the specific problem of deconvolution and its related problems of noise removal and data linearization, and established methods for evaluating the results of the techniques developed. Phase A occupied a five and one-half month period, and Phase B required six and one-half months. Figure 15 is a work flow diagram which illustrates the approximate order of the project work tasks.

2.1 PHASE A ACTIVITIES

Phase A activities were intended to provide the basic software routines and operational procedures that would be needed for carrying out the tasks of Phase B once image processing hardware became available. Three general work areas were addressed:

- To develop compatability guidelines
- To develop utility software
- To investigate techniques for noise removal.

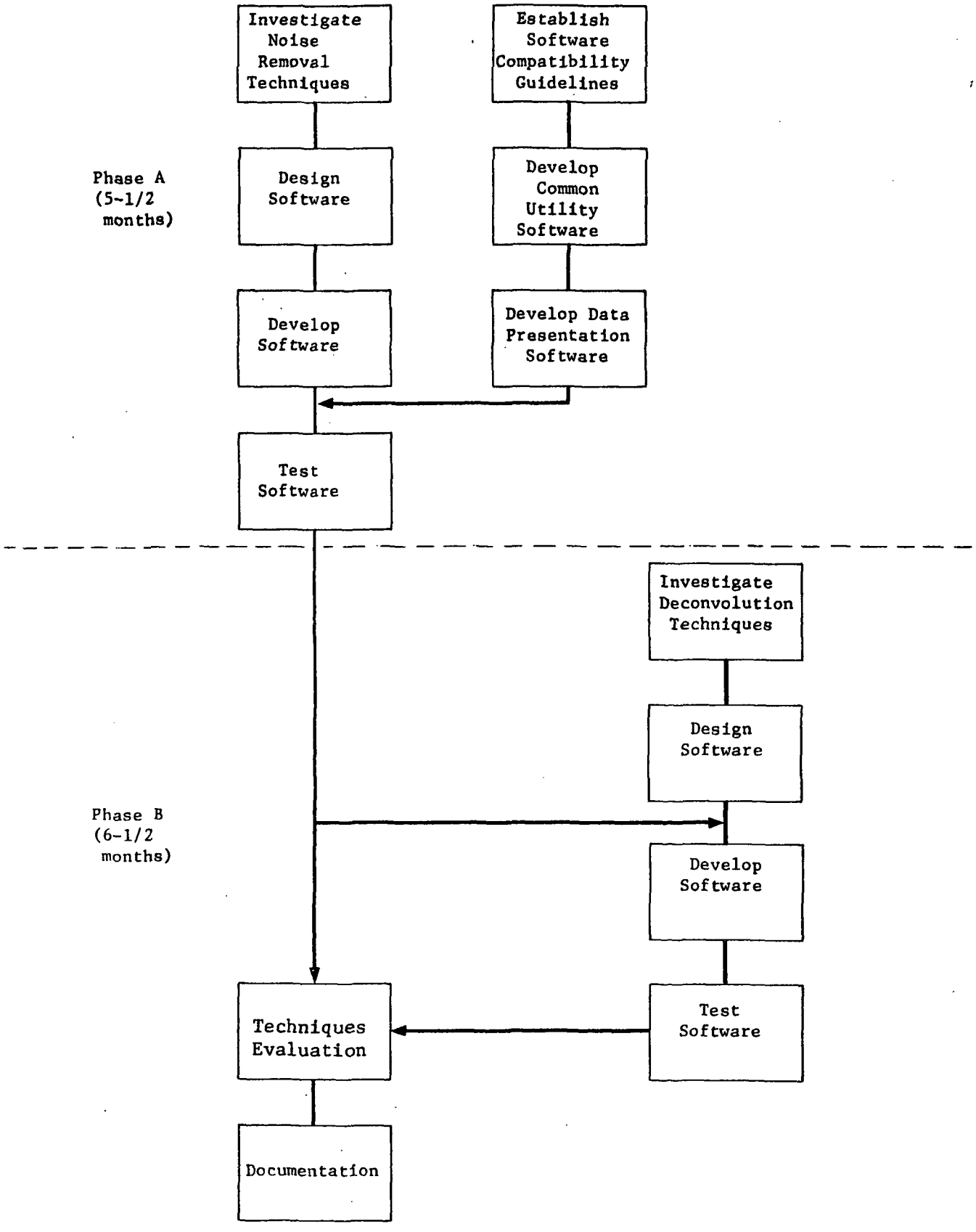


Figure 15 - Work Plan and Performance Schedule

2.1.1 Compatibility Guidelines

Preliminary information on photo scanning and display equipment enabled the project team to establish a set of compatibility guidelines for handling the S-056 image data. For example:

- Image data would be transferred from photo-scanning equipment to 7094 computer on magnetic tape. This tape would be written in standard IBM 7-track format and each picture scan value would be represented as a six-bit byte, packed six bytes per word on the tape.

- Image data would normally be converted from scanner input format to computer format with each picture scan value occupying one computer word in standard FORTRAN format.

- All software routines would be written in FORTRAN IV so as to be easily transferrable to another computer.

- Subroutines would be designed to be independent of specific tape drives for input, output, and scratch storage so that tape assignments could be made automatically by the operating system.

- Image data frame sizes would normally be a square array which is a power of two.

- Frame sizes and picture element locations would normally be specified by two numbers -- the first corresponding to the line or vertical dimension, and the second corresponding to the column or horizontal dimension.

- MSFC Library routines would be used in software design wherever applicable.

- Image processing operations would be performed in integer arithmetic except where truncation is a factor in which case floating point arithmetic would be used.

- All image output data would be reformatted from computer format to photo-display format by converting each picture value from computer format to a six-bit byte and packing six bytes per words.

- Image output data would normally be produced with record lengths of 1024 bytes. A full frame of image data would contain 1024 records.

These guidelines were not binding in all cases, but they did serve to establish a standard for operation which greatly improved project efficiency.

2.1.2 Utility Software

The importance of limiting the computer programming effort so that available resources could be focused on the problems of developing techniques for restoring S-056 photographs was recognized early in the project. The importance of being able to make changes to computer runs with a minimum of programming effort was also understood. It was expected that much of the development effort would be a "cut and try" process of applying a technique as a trial, making an evaluation, modifying the approach and making another run. It was obvious that such an iterative process would require considerable software flexibility. In order to provide computer software with the required flexibility, SDC developed an Image Data Processing System called IDAPS. IDAPS is designed to operate on the MSFC 7094 computer for development, test, and evaluation of techniques for processing S-056 image data. It provides:

- A framework or standard for implementing image data processing applications,

- A simplified means for making image processing runs without a working knowledge of computer programming, and

- A streamline means for setting-up and running any desired combinations of image processing applications without operator interaction.

IDAPS is built around a system language which consists of basic "operators" which when interpreted by the system, cause the system to construct the necessary parameters for each application, make all necessary tape assignments, set up needed print formats, print detailed instructions to the computer operator on where to load input data and where to retrieve the output, and call appropriate application subroutines in the proper order. Using IDAPS, programming time has been cut drastically, and time lost in conventional deck setup and "debug" operations has been largely eliminated. A more complete description of IDAPS, an operator's users manual, and descriptive data on all IDAPS subroutines is provided as Volume II of this report.

2.1.3 Noise Removal

Preliminary evaluation of some S-056 test photographs early in the project called attention to the problems that may be expected as a result of noise. Consequently various noise removal techniques were studied during the Phase A effort to isolate those which were most useful for S-056 application. Several noise removal techniques which showed promise for S-056 application were tested to determine their suitability for use in conjunction with the deconvolution process during this phase of the contract.

2.2 PHASE B ACTIVITIES

Phase B activities got underway when photo-scanning and recording equipment were installed at MSFC. With the new equipment, photographs could be scanned and converted to computer format, the computer processed data could be displayed on a CRT for "quick-look" review, and the processed pictures could be reproduced on photographic film as a permanent record photograph.

Phase B activities centered around the process of deconvolution and the noise removal and data linearization techniques needed to support deconvolution.

Another important part of Phase B was the effort devoted to technique evaluation. Methods had to be devised for determining the extent of improvement (if any) resulting from the application of a technique. The deconvolution technique development and evaluation efforts were carried out in parallel in Phase B.

2.2.1 Deconvolution

The development of deconvolution techniques for restoring S-056 photographs has been the primary task of this project. Not only was it important to develop deconvolution software but it was also important to find ways of reducing the effects of noise and non-linearity in the image data and to determine to what extent the many variables of the deconvolution process might be manipulated in order to reduce those effects. The approach used in this effort, the results obtained, and the conclusions and recommendation which resulted are documented in Section 3 and 4 which follow.

2.2.2 Technique Evaluation

The evaluation procedure used in this project involved the iterative application of the technique in question to a suitable test image in a number of trail runs. With each application, a single technique variable was changed and all other variables held constant. After several such test runs, the results (normally in picture form) were displayed together, and the resulting display array was analyzed to determine optimum values for the technique variable, to identify trends and to make generalizations about the effect of the variable on the technique, and to set up new evaluation series.

The procedure of iterative testing of image processing technique variables was used throughout the technique development effort.

SECTION 3. TECHNIQUE DEVELOPMENT

Even though the design of the S-056 telescope represents an advance in the "state-of-the-art" in X-ray astronomy, the images which the telescope produces will still be severely distorted. The purpose of this project has been to develop methods of digital image processing to manipulate these S-056 images in order to improve their quality. Because image processing considerations did not influence the original design of the S-056 telescope this work has concentrated on developing methods of image correction which could be applied to the experiment photographs after they are returned from space. Figure 16 illustrates the situation of this work.

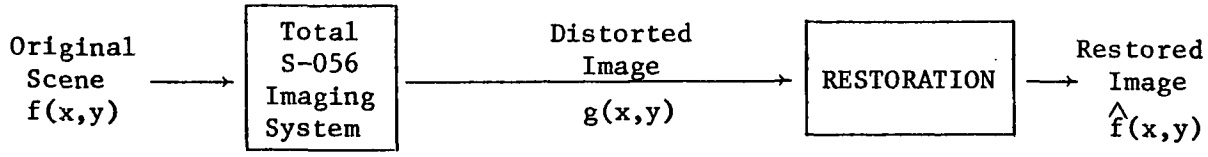


Figure 16 - Image Restoration Project Work Situation

The original scene represents an ideal image (f(x,y)) which is the input to the S-056 imaging system. If S-056 were a perfect photo-optical system, and if no external alterations were introduced into f(x,y) before entering the S-056 system, then the pictures produced by the telescope would be a perfect representation of the original scene. Because of the physical limitations of the S-056 system, the image data is distorted and noise and other aberrations are introduced. This results in a distorted image (g(x,y)). Figure 17 represents a simplication of the degradation process which takes place in the S-056 imaging system. In general, however, the degrading system would be very complex and absolute restoration of the distorted image g(x,y) to its original form would be impossible but, even in the worst cases, considerable improvements can be made in the distorted image.

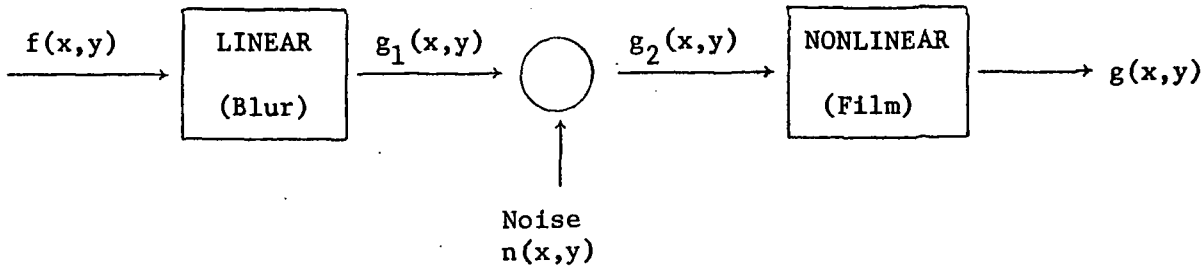


Figure 17 - S-056 Imaging System Degradation

The primary cause of the linear degradation is the blurring caused by image convolution. Although the noise (n(x,y)) is shown entering the system at a discrete point, it is actually introduced throughout the system. Severe nonlinearities may be introduced by the photographic film and further nonlinear degradations and noise may be added as a result of the scanning process which is necessary to convert the film for computer processing.

By applying appropriate image processing techniques to the distorted image (g(x,y)) it is possible to restore g(x,y) to a much more accurate representation of the original scene ($\hat{f}(x,y)$). With respect to the peculiar needs of the S-056 data, deconvolution appears to be the most powerful tool available for image restoration.

3.1 PRINCIPLES OF DECONVOLUTION

If the S-056 optical system has an impulse response of $h(x,y,\alpha,\beta)$ then the output $g_1(x,y)$ of the major linear element shown in Figure 17 can be expressed by

$$g_1(x,y) = \int_{-\infty}^{\infty}\int_{-\infty}^{\infty} h'(x,y,\alpha,\beta)\ f(\alpha,\beta)\ \ d\alpha d\beta. \qquad (1)$$

Preliminary mathematical and laboratory analysis of the S-056 telescope optics indicate that the system is not completely linear, however, the assumption of system linearity for the purpose of image restoration should lead to significant improvements in the S-056 images.

If the linear system is shift-invarient then the superposition integral (1) can be written as a convolution

$$g_1(x,y) = \int_{-\infty}^{\infty}\int_{-\infty}^{\infty} h(x-\alpha,y-\beta)\ f(\alpha,\beta)\ \ d\alpha d\beta. \qquad (2)$$

The S-056 optical system is not shift-invarient over its entire field of view, but it is sufficiently shift-invarient over localized areas to permit this simplification.

The mathematical operation described by Equation (2) is the mathematical expression for convolution in two dimensions. If two-dimensional Fourier transforms of each of the components of Equation (2) can be obtain, the convolution operation may be described as

$$G(u,v) = H(u,v) \cdot F(u,v) \qquad (3)$$

where G, H, and F are the two-dimensional Fourier transforms of g, h, and f, respectively, and u,v are spatial frequencies.

The task of image restoration with respect to the linear block shown in Figure 17 is to determine f(x,y) given $g_1(x,y)$. This can be accomplished by dividing (point-by-point) both sides of Equation (3) by H(u,v) and then taking the inverse two-dimensional Fourier transform of the result

$$f(x,y) = F^{-1}\left[\frac{G_1(u,v)}{H(u,v)}\right]. \qquad (4)$$

That is, the effects of the linear distortions resulting from the S-056 optics may be eliminated (under ideal circumstances) by deconvolution and deconvolution becomes a simple point-by-point division in the frequency domain. With the introduction of the fast Fourier transform, the transform approach to digital deconvolution has become more efficient than the direct solution of Equation (2). The principles of the fast Fourier transform are briefly outlined in Appendix A.

The restoration technique exemplified by Equation (4) is not as simple as it seems. The S-056 images are recorded nonlinearly on photographic film and noise is present in every step of the process from telescope optics to developed photographic image. Also, the device used to convert the photographic images to digital images introduces both nonlinearities and noise. Furthermore, because of noise, or error in determining the system PSF, the function H(u,v) in Equation (4) may be equal to zero at some point where $G_2(u,v)$ is not. Therefore, Equation (4) cannot be blindly applied with the assurance of getting desirable results. Instead, the deconvolution process must be carefully controlled and the conditions under which it may be applied must be thoroughly understood if it is to be useful as a tool for image restoration.

3.2 CONDITIONS FOR SUCCESSFUL DECONVOLUTION

The deconvolution process loses its apparent simplicity when the conditions under which it may be applied are considered. The factors of noise and nonlinearity, the difficulty of accurately determining the system point spread function and the process of accurately representing the picture data in computer recognizable form all combine to make deconvolution of real data a formidable task. An understanding of the conditions for successful deconvolution is, therefore, essential.

Four primary considerations for applying deconvolution to S-056 image data have been identified:

- Image Conversion Accuracy
- Film Data Linearity
- System Noise
- System PSF

3.2.1 Image Conversion Accuracy

The accuracy with which the image data may be described in digital form depends in large measure on the size of the aperture used for scanning, the separation between sampled points, and the number of quantization levels used in representing

film densities. Films used in this project were scanned with a microdensitometer which provided an option of scanning with a 12.5, 25, or 50 micron aperture with edge-to-edge spacing. The microdensitometer quantized the scanned image to 64 levels-of-gray.

Image data is quantized to one of 64 levels as an exponential function of film density. The maximum density is chosen as either 2D or 3D, when D is the logarithm of film opacity. Microdensitometer output is recorded on magnetic tape.

Hardcopy was provided by a film writing device which modulates a spot of light to expose Kodak Shellburst film through either a 12.5, 25, or 50 micron square aperture. This device accepts input image data (quantized to 64 gray values) from magnetic tape. A CRT thermoplastic display device provided a "quick-look" of data prior to or in place of producing a film hardcopy output.

Because the image conversion devices interface with the computer through magnetic tape and because the image data format of the devices is different from standard computer format, it was necessary to develop software routines for changing the data formats. Several IDAPS operators were developed for this purpose: CHANGE FORMAT, DISPLAY FORMAT, MULTIPLE DISPLAY, etc., (see Volume II for more details).

3.2.1.1 Sampling Resolution - In general, the sampling rate (aperture size and separation) should be at least twice the highest spatial frequency present in the original, und storted, noiseless scene. If, however, the image is recorded on film with grain size larger than the sampling aperture the sampling rate may be reduced proportionately. In order to reduce processing time, image data should be sampled at the lowest rate which adequately describes the image.

3.2.1.2 Quantizing Resolution - Just as it is necessary to sample a picture at a sufficient rate, it is also necessary to quantize the image to an adequate number of quantization levels in order to accurately describe the data.

Excess quantization levels should be avoided in order to hold processing time to a minimum, but no simple formula can be applied to determine what the minimum quantization requirement is.

In order to gain sufficient experience so that a subjective evaluation of the effects of quantization on the deconvolution process could be made, a study was performed under carefully controlled conditions to isolate the effects of quantization from all other influences. In order to eliminate film and scanner distortions, the investigations were performed in a computer environment and in floating point arithmetic, except for the quantization of the distorted images. A test image was generated consisting of a black square (32 x 32 picture elements) on a white field (64 x 64 picture elements). This image was convolved (blurred) with a cone shaped point spread function. The distorted image was then quantized to 64, 128, 256, and 512 levels and each quantized image was deconvolved (using Equation (4)) with the same point function used to obtain the blurred image. The results of this study are shown in Figure 18.

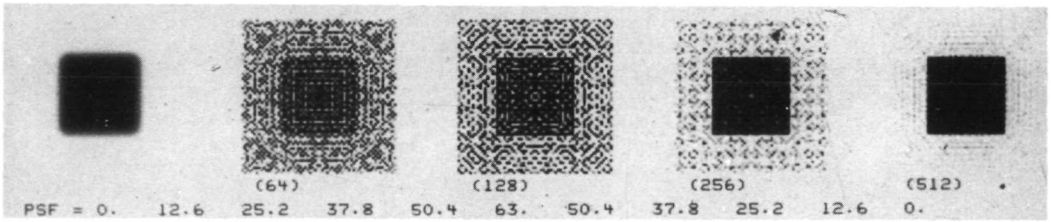


Figure 18 - Study of the Effects of Quantization on the Deconvolution Process

The image on the left is the blurred black square; the images to the right are the results of deconvolving the blurred images which have been quantized to 64, 128, 256, and 512 levels. It may be observed that in no case does deconvolution restore the image to the perfect black square, but improvement does occur as more and more quantization levels are used to represent the intensities of the sample points of the blurred image.

Quantization accuracy is not the only major variable present in the preceeding experiment. The amount of blurring present in the distorted image will greatly affect the quantization accuracy required for successful deconvolution. To test the strength of this dependency, the previous experiment was repeated with different degrees of blur. The results are shown in Figure 19.

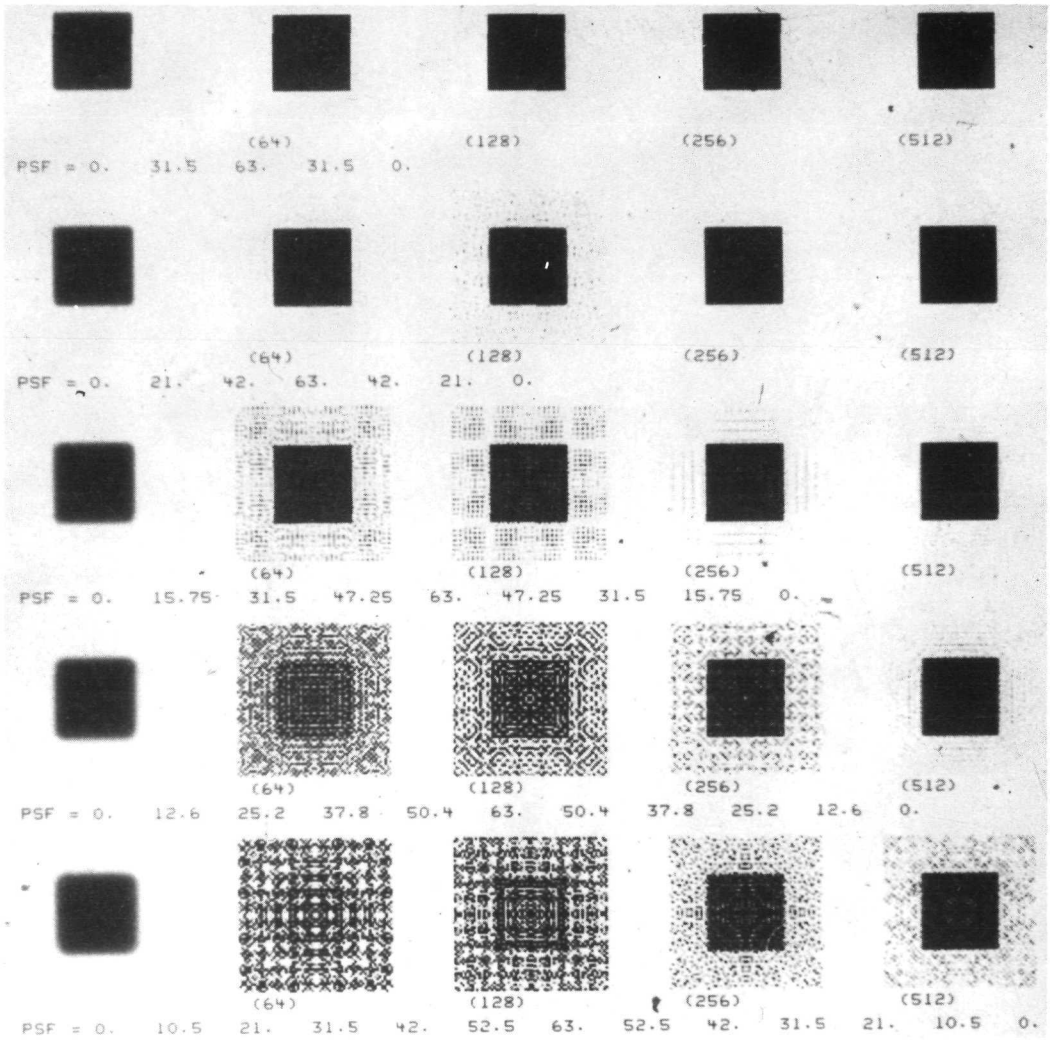


Figure 19 - Study of the Effects of Quantization and Extent of Blur on the Deconvolution Process

The left column of images depicts the black square blurred with successively larger point spread functions. The profile of the PSF corresponding to the burred image is printed immediately below the images of each set. The test pattern chosen for this study (the pattern presents high gradients at the edges) and the degree of blur to which it is subjected constitutes an unusually severe test of the quantization requirements of the deconvolution process, but from the study it is possible to postulate that as blur becomes more severe, the requirements for quantization accuracy increase.

The deconvolution process in each of the previously described experiments was a direct application of Equation (4). A more thorough investigation of the images shown in Figure 19 reveals a repetitive pattern in many of the images. Even though the black square test image is a simple geometric shape which will tend to produce symmetric patterns, many of the patterns present in Figure 19 appear to result from overamplification of certain frequency terms. If H(u,v) in Equation (4) (the two-dimensional Fourier transform of the PSF) approaches a magnitude of zero at some point and the corresponding image transform term remains relatively large, then the value $G_1(u,v)$ at that point will be amplified by 1/H(u,v) and the resulting number may dominate all other frequencies in the array. In such a case, the inverse transform of $G_1(u,v)/H(u,v)$ will exhibit repetitive patterns like those in Figure 19.

In order to test the theory that the patterns of Figure 19 were the result of frequency component misamplification and also to test a simple means for reducing the effect, a new test series was run. In this series, the procedure of the previous study was repeated, except that the value of $|1/H(u,v)|$ was not allowed to exceed 30,000. The results are shown in Figure 20. Compare the results of this study with those shown in Figure 19. Thus it may be observed from Figure 20 that limiting the amplification of frequency terms reduces the quantization requirements of the deconvolution process. Although the generalization that as the level of blur increases, the number of quantization levels required increases still holds, the level at which significant improvement is produced through deconvolution is lower for this form of controlled deconvolution than for the straight application of Equation (4).

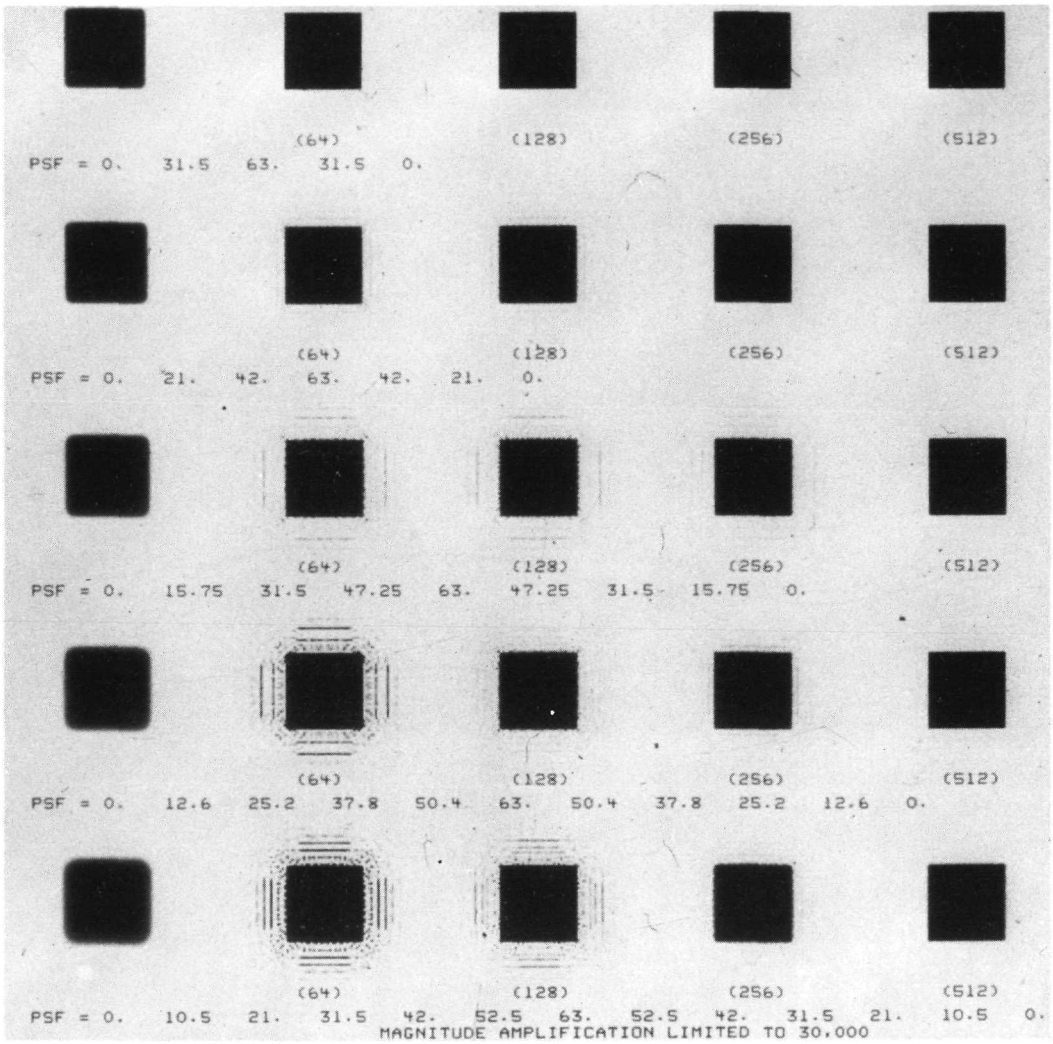


Figure 20 - Application of Frequency Term Amplification Limiting to Deconvolution of Images with Varying Levels of Blur and Quantization Rate

3.2.2 Film Data Linearity

It was pointed out in Section 1 that the S-056 image blur could be described as the mathematical convolution of an image light intensity array with a system point spread function. The phrase "light intensity array" bears special

significance to the deconvolution technique because it means that deconvolution must operate on light intensities -- not film densities. Photographic film records the light intensity which strikes its surface as a corresponding film densities. This recording process is generally nonlinear. Further nonlinearities are introduced by the scanning microdensitometer as a result of instrument imperfection. Before the deconvolution process can be satisfactorily applied to a blurred photograph, the nonlinearities must be corrected, so that the digital image data is in terms of light intensity. The success with which such corrections may be made depends on the accuracy of quantization and the accuracy with which the film and scanner characteristics are known and described.

Two data curves are of interest -- the film characteristic curve, and the scanner conversion curve. The conversion characteristics of photographic film are normally presented as a semi-logarithmic plot of light intensity values versus film densities. Such a characteristic curve is called the film D Log_{10} E curve. Figure 21 is a representative (of normal photographic film) film D Log_{10} E curve. This curve has three fairly well-defined regions: a linear region (B to C); a lower nonlinear "toe" (A to B); and an upper nonlinear "shoulder" (C to D). From such a curve, a number of important film characteristics may be determined: the sensitivity or speed of the film; the contrast or dynamic density range; the latitude or useful density/energy range of the film; and most importantly, the manner in which high intensity will be represented as film density. The slope of the linear region of the curve is called the film "gamma" and is a measure of the rate of density change with respect to applied light energy.

The scanner conversion curve is a plot of gray scale value versus film density and includes all effects of the microdensitometer light source, photomultiplier, and electronics. There are two general categories of film corrections -- linearization, and enhancement.

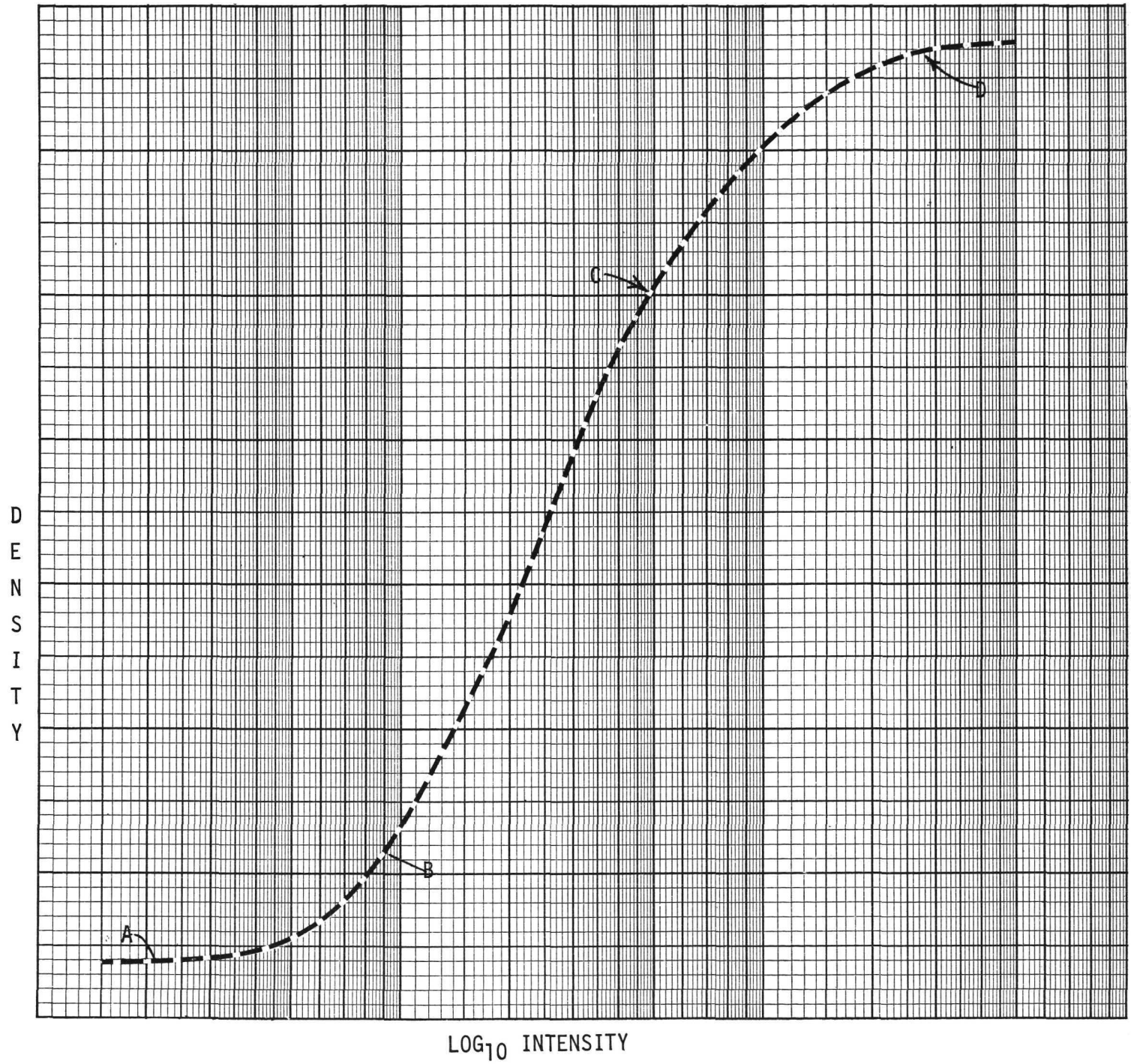


Figure 21 - Characteristic D Log_{10} E Film Curve

3.2.2.1 Linearization - In order to prepare S-056 film data for deconvolution it must be corrected to compensate for both film and scanner nonlinearities. To do this, accurate data must be available with which to describe the film, and scanner characteristics. During this project, no such information was available for the scanner and film curve data was available in only very preliminary form. Nevertheless, computer software which will be capable of correcting for the nonlinearities when the characteristics become available was designed and tested. This software routine is included in IDAPS and is referred to as the "INVARIENT ALTER" operator (see Volume II).

3.2.2.2 Enhancement - Aside from the corrections needed to prepare an image for deconvolution the IDAPS operator INVARIANT ALTER may be used to make an image more visually attractive even though such alterations may introduce even more severe nonlinearity. Three typical forms of image enchancement are: correction for under-exposure; correction for over-exposure; and correction for fogging or low contrast.

It is normally desirable to expose film so that film densities lie along the linear portion of the D Log_{10} E curve with an average gray "operating point" in the center of the linear region. If for some reason, insufficient light is passed to the film, an under-exposed or "thin" film will result. This effect is illustrated in Figure 22a. In this case, the photograph of Abraham Lincoln appears light and very "washed out". If, on the other hand, the image is over-exposed, the picture will be very dark or "dense" as seen in Figure 22c. In the first case, exposure took place along the "toe" of the D log_{10} E curve while in the second, along the upper "shoulder". In both cases, only eight quantization levels were detectable with the available microdensitometer, but by redistribution of the eight density levels of each of the two photographs a significant enhancement of the original pictures was obtained as seen in Figure 22b and 22d, respectively.

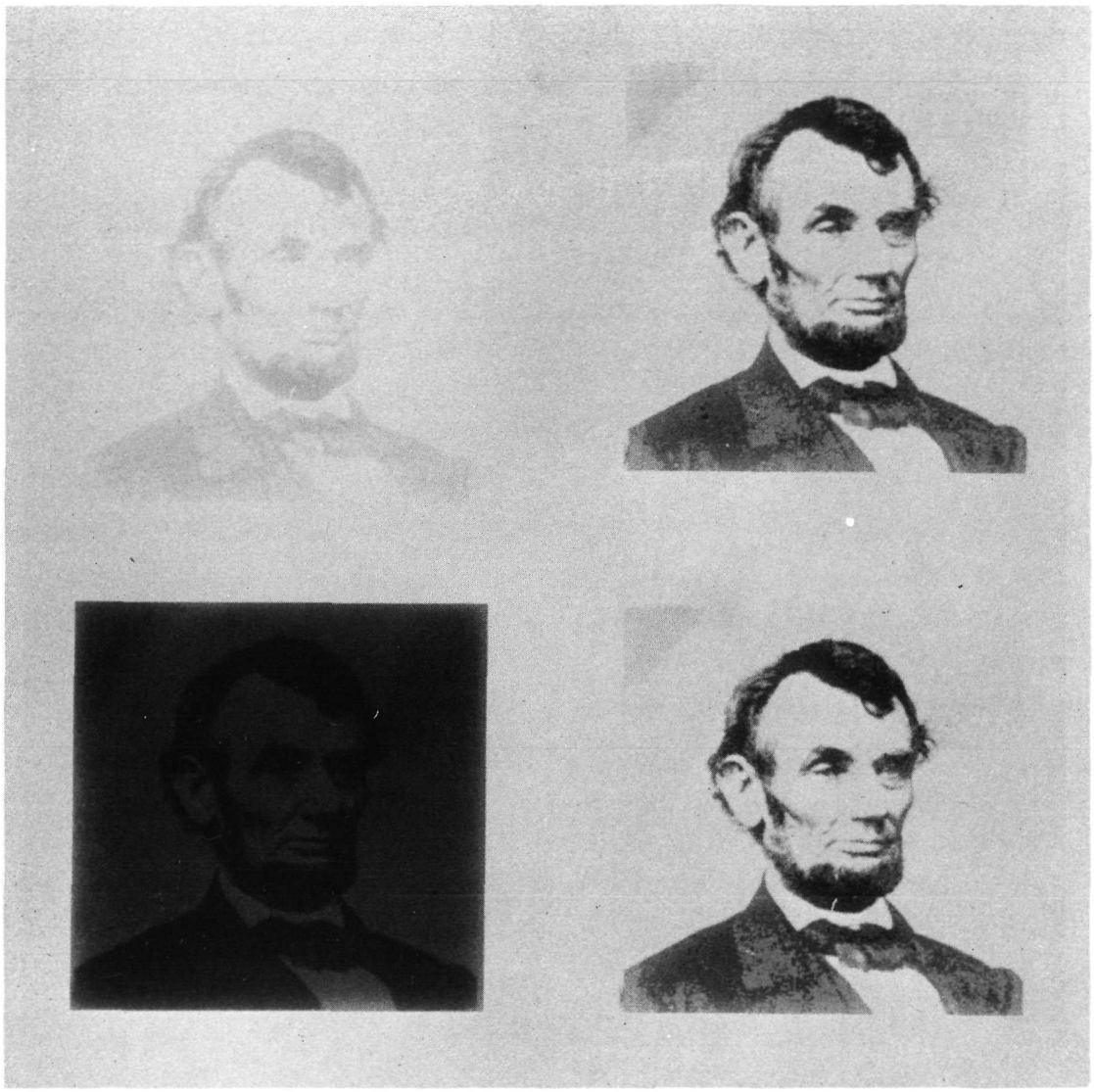


Figure 22 - Illustration of Image Enhancement
(a) Under Exposed (upper-left); (b) Enhancement of (a) (upper-right); (c) Over Exposed (lower-left); (d) Enhancement of (c) (lower-right)

Factors other than incorrect exposure may degrade the appearance of a photograph. Poor lighting conditions may produce a scene of low contrast, and unless a film with a compensating gamma is chosen and properly exposed, the resulting image will have low contrast. A similar problem may result from fogging. Fogging can be caused by improper storage, exposure to certain chemical environments,

or stray radiation. Figure 23a illustrates the result of film fogging. Contrast is poor, and even the lightest areas in the picture are a medium gray. The scanned data from this picture exhibited gray levels between 21 and 50. A redistribution of the 30 available gray levels (to levels in the range of 0 to 63) produced the picture in Figure 23b.

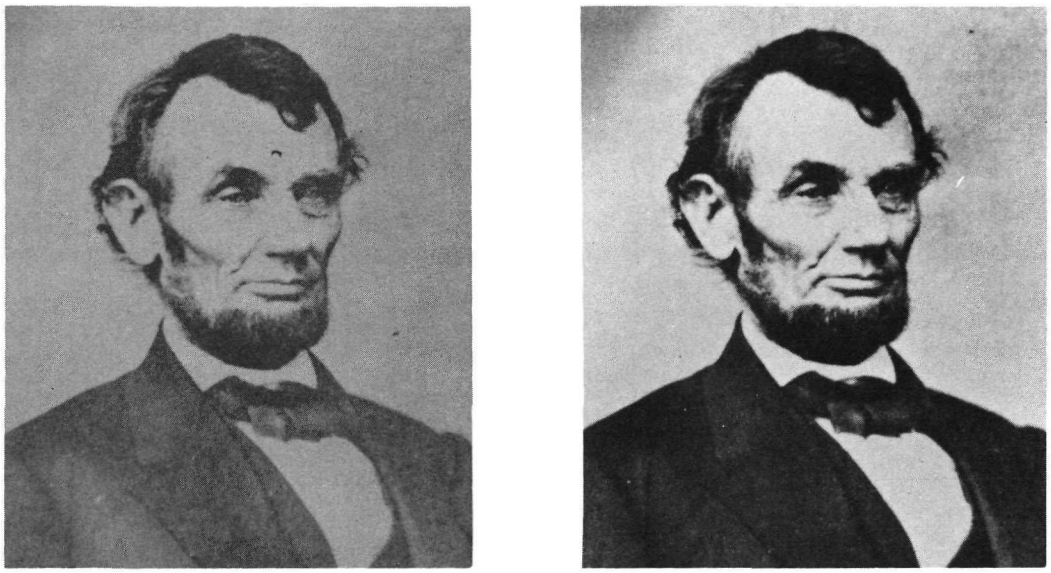


Figure 23 - Enhancement of a Fogged Image
(a) Fogged Image (left);
(b) Enhancement Results (right)

The form of redistribution which will yield the most desirable enhancement is difficult to determine. Many extensive studies have been made in the area both theoretically and through subjective evaluation. Wilder (1) has compiled the results of these studies and has attempted to relate a mathematical model to the results of the subjective evaluations. A general consensus of opinion is that a curve which maps intensity to film density and lies somewhere between a square root curve and a cube root curve yields the best image for visual analysis.

In order to take advantage of visual properties of the eyes and eliminate the data set required by INVARIENT ALTER, an IDAPS operator called SCALE was developed. SCALE determines the minimum and maximum gray levels present in a computer

image and maps the original floating point gray values between prespecified upper and lower limits into new values according to a (1) square root curve, (2) cube root curve, (3) logrithmic curve, (4) square curve, or (5) linear curve. This operator is primarily designed to manipulate floating point data such as output by the deconvolution operation. The linear curve operation, however, works quite well on quantized data.

3.2.3 Noise

Noise is a major problem in image restoration. The presence of noise severly affects the quality of an image. Even for the case of a well-behaved PSF, the noise level associated with the restored image may be so high as to make the image meaningless. Indeed, deconvolution may not even be possible until the noise level of the blurred image has been reduced.

There are two general classes of noise: random and correlated. Random noise may arise from stray radiation, film granularity, or the photomultiplier. Correlated noise may arise from film scratching, film scanning, or from the deconvolution process itself when random noise is present in the input image. The word correlated as used here means that the amount of noise at one point in an image is related to the amount of noise at other points and does not necessarily imply (or exclude) a correlation between the scene and the noise. Random noise is the most difficult type to remove from the recovered images.

3.2.3.1 Random Noise - One of the most efficient ways of reducing random noise is by multiple frame averaging. If multiple frame exposures of the subject are registered with respect to each other, then a simple point-by-point averaging of the individual images will produce a new image which has a significantly reduced noise level. This operation is represented mathematically by Equation (5).

$$g'(x,y) = \frac{1}{m} \sum_{j=1}^{m} g_j(x,y) \qquad \begin{matrix} x = 0,1,\ldots, N \\ y = 0,1,\ldots, N \end{matrix} \qquad (5)$$

In a slightly more sophisticated scheme, the points of a particular location are first averaged, then any point which differs significantly from the average is thrown out and the remaining points are reaveraged. Another approach is to sum corresponding points of several images and then process the resulting image of increased quantization levels to obtain similar results. A fourth method which is more efficient for certain types of distortions is amplitude and phase averaging (2). In this situation each of the multiple frames is corrected for film nonlinearities and then registered with respect to the other frames. A complex two-dimensional Fourier transform of each image is computed and converted into amplitude and phase form, and the multiple frame transforms are averaged for each spatial frequency, as shown by Equation (6).

$$\Phi'(u,v) = \frac{1}{m} \sum_{j=1}^{m} \Phi_j(u,v)$$

$$A'(u,v) = \frac{1}{m} \sum_{j=1}^{m} A_j(u,v) \qquad (6)$$

$$u = 0,1,\ldots, N$$

$$v = 0,1,\ldots, N$$

$\Phi_j(u,v)$ is the phase of the Fourier transform of $g_j(x,y)$

$A_j(u,v)$ is the amplitude of the Fourier transform of $g_j(x,y)$

During periods when the S-056 telescope will be operating in the "active" mode, multiple exposures will be made in a short period of time. These images should be suitable for multiple frame averaging. Before averaging such exposures, however, they must be accurately aligned or "registered" so that corresponding image features are addressable at the same picture element location in the scanned image arrays. Such registration may be accomplished with specialized hardware or it may be accomplished in the computer with the proper geometric manipulation and comparison software. Specialized hardware was not available to the project team and development of adequate computer software for machine

alignment would have entailed an effort which could not be accomplished under the present scope of the contract. Computer software was developed, however, to average the multiple frames after they have been registered. The IDAPS operator for multi-frame averaging is AVERAGE. A combination of AVERAGE with other IDAPS operators will allow all of the multiple frame averaging procedures described previously to be carried out under IDAPS.

In order to test and evaluate the multiple frame averaging techniques a computer generated test pattern was used. Five images each consisting of a black square (32 x 32) on a white field (64 x 64) were generated. Then random noise with a uniform discrete distribution between -16 and +16 was added randomly to 4% of the data elements of each image. The first five images of the first row of Figure 24 are the resulting noisy, blurred images. Each blurred, noisy image was deconvolved using Equation (4) and the original degrading point spread function. The resulting deconvolved images are shown as the first five images of the second row of Figure 24.

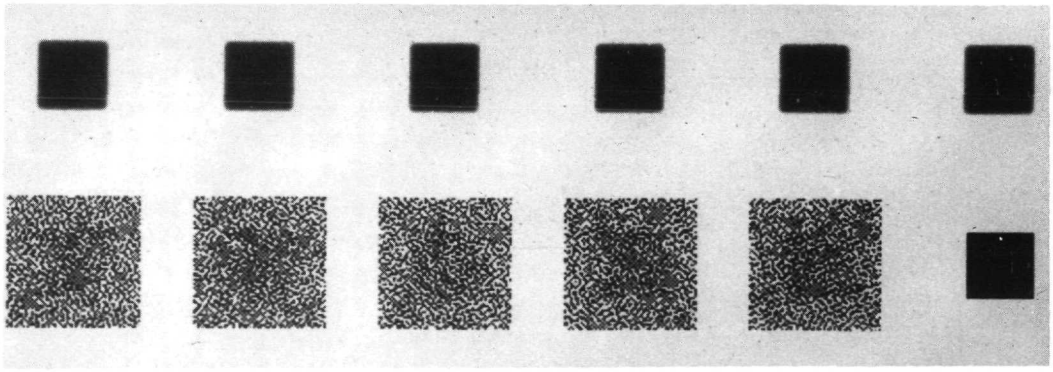


Figure 24 - Study of the Effectiveness of Multiple-Frame Averaging for Noise Reduction Prior to Deconvolution

It is clear that straightforward deconvolution cannot be successful in the presence of such noise as is exhibited in the first five pairs of images. The next step was to average the five noisy black squares and deconvolve the results. The last image of the first row of Figure 24 is the average of the five test patterns, and the deconvolution result is directly below it. The results of this study and other similar investigations point out the need for a complete set of software for multiple frame averaging. The software should be able to perform the geometric corrections, manipulations, and comparisons required for frame registration. Multiple frame averaging is also an efficient method for removing film blemishes and scratches.

Spatial filtering is sometimes an effective means for dealing with random noise provided the dominant noise frequencies are somewhat disjoint from the image frequencies. Proper application of the IDAPS operators FFT, CENTER, LOG MAGNITUDE, and DISPLAY can produce a Fourier transform of the image ($\log_{10}$ magnitude) for visual analysis. In this transform the DC term is centered and frequencies increase toward the edge of the transform. Phase information is handled in a similar manner. Figure 25 illustrates the use of this approach to spatial filter design.

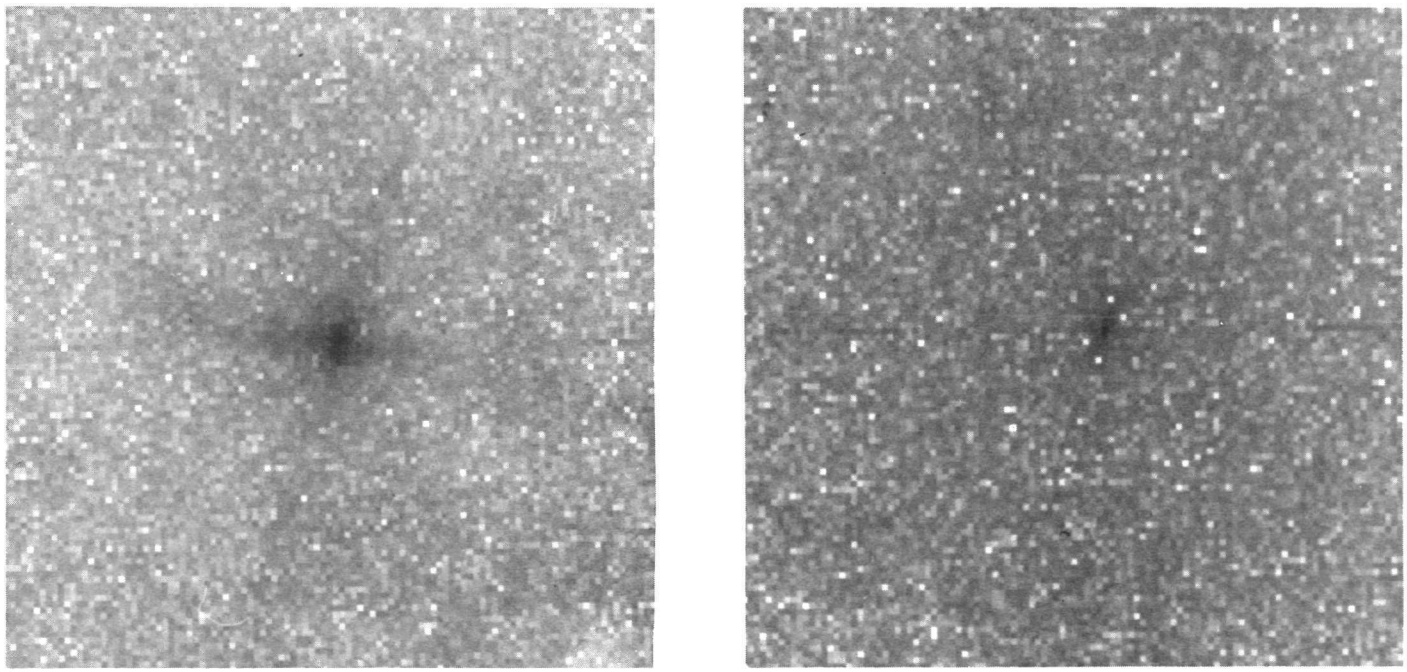


Figure 25 - Display of the Logarithm of Fourier Transform Magnitude Terms: (left) Transform of Figure 7, (right) Transform of Figure 7 Background Only

The left hand picture is the magnitude ($\log_{10}$) of the transform of the S-056 image presented in Figure 7. The picture on the right is the transform of just the background noise of the same image. The difference of the two pictures (the elongated dark area in the center of the left hand picture) accounts for most of the transform information of the noiseless blurred image. The speckled background is largely due to noise. By setting those terms to zero and reconstructing the image from the remaining terms, much of the noise in the S-056 photograph may be eliminated.

Another effective method for reducing the effects of random noise in an image is point averaging. Point averaging, in its most rudimentary form, is simply the replacement of a point which differs significantly from its neighboring points with the average of the neighboring points. A slightly more sophisticated procedure is implemented by the IDAPS operator INTEGRATE. INTEGRATE allows the specification of the amount by which a point can vary from the average of its neighbors before it is adjusted and specification of the percentage of the adjustment. This algorithm has been evaluated and found to improve the visual qualities of an image whenever the random noise present in the image effects a small percentage of the image points by a significant amount.

In the presence of noise it is not possible to obtain a perfect restoration of an image. Harris (3) has shown that by sacrificing some resolution in the restored image, the noise level in the restored image may be greatly reduced. In this approach, which is a form of point averaging, the image is first convolved with a "noise suppressing point spread function", then deconvolved with the imaging system point spread function. The resulting deconvolved image will have less resolution but will contain less noise. IDAPS operators CONVOLVE or FORCON provide the means for this form of point averaging. Thoughtful consideration will reveal that the cumulative effect of these two operations is equivalent to a deconvolution of the original blurred image with an adjusted point spread function. Unfortunately there is no way to determine the "noise suppressing PSF" directly. An iterative, subjective evaluation of a noisy system's PSF will lead not to the true system PSF but to an optimum noise suppressing PSF.

3.2.3.2 Correlated Noise - Correlated noise is generally more easy to deal with than random noise. Such noise may result from image scanning, from improper selection of the PSF, or from noisy deconvolution and must be eliminated as part of the restoration effort. A direct analysis of an image can sometimes provide clues of a dominant noise characteristic but more often an analysis of the Fourier transform of the image is required. This may be done by preparing a display of the image transform as outlined in the previous section. If an image is distorted by strongly correlated noise, the magnitude of the image transform will display a dark region on the transform display, centered about the location of the offending frequency.

Once the dominant frequency of periodic noise is isolated it may be removed with a form of two-dimensional band-reject filtering. The specification of the filter at specific transform frequencies ($\omega a, \omega b$) would be desirable but is not presently practical. Instead, a scheme has been devised for selectively attenuating entire frequency bands. The noisy image is first transformed, centered, and displayed in the manner described previously. The IDAPS operator GRADIENT is then used to modify transform terms as a function of their radial distances (frequency magnitude) from the center of the array. The effect is to produce a doughnut shaped, two-dimensional filter in which dominant noise frequencies are located. Figure 26 illustrates the effect of band-reject filtering on an image distorted by correlated noise. The upper left is the original image of Lincoln, immediately to the right is the same image corrupted by dominant presence of several frequency terms. The remaining frames reflect the images resulting from band-reject filtering as the rejection band is moved from highest to lowest frequencies. As the filter approaches the dominant noise frequency the distorted image improves and becomes clear and then distorts again as the rejection band moves on past.

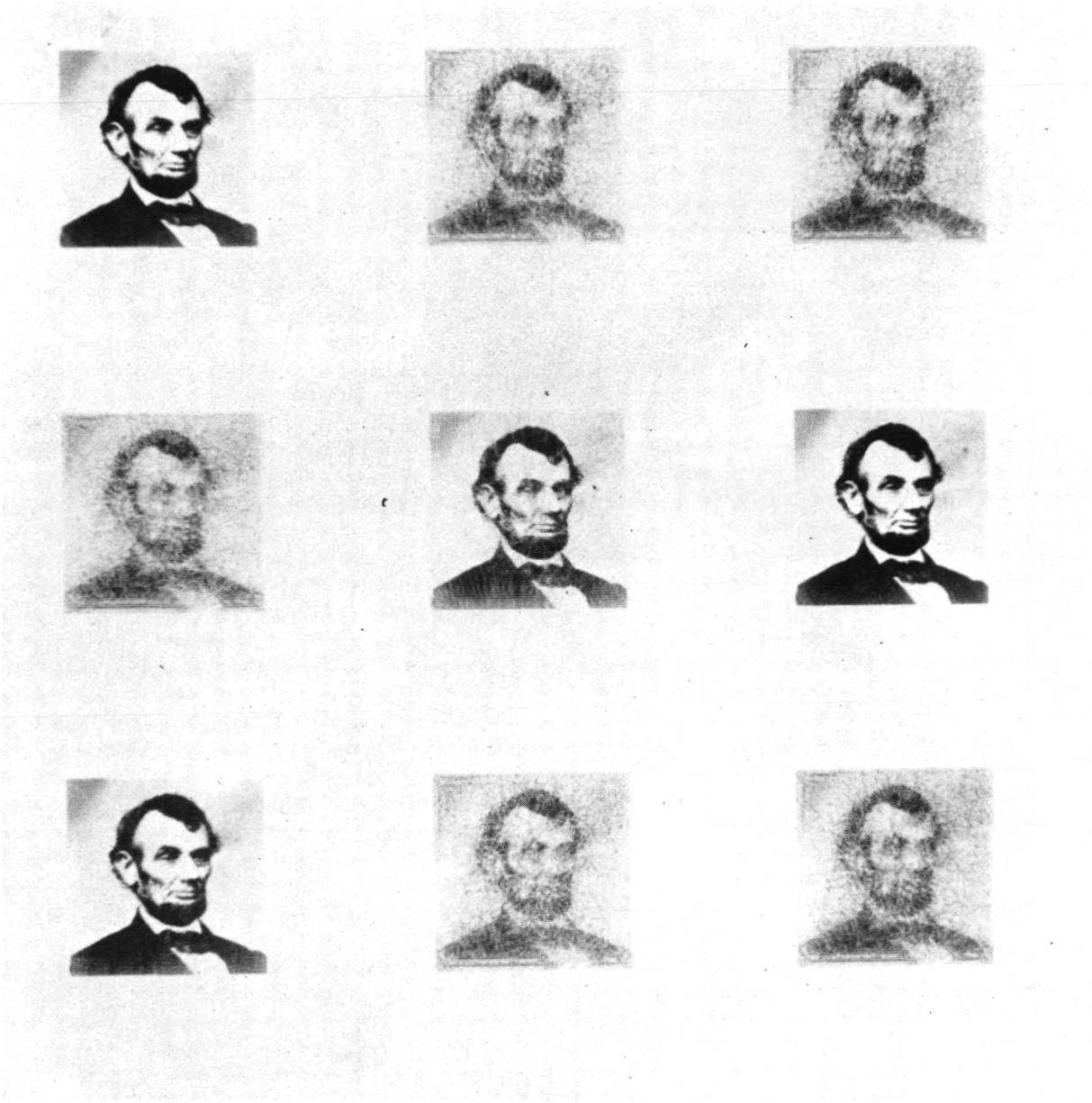


Figure 26 - Illustration of the Use of Band Reject Filtering for the Removal of Correlated Noise

3.2.4 System PSF

There are numerous methods of estimating system point spread functions. The methods available have not been completely tabulated in any one source but Huang et.al. (4) have described four major catagories. A slightly modified list follows: (a) measurement of degrading system, (b) theoretical analysis, and (c) analysis of flight images.

(a) If the image degrading system is available to the image processor then laboratory measurements may aid in the estimation of the system point spread function. A typical approach is to record the image resulting from a point source, line, or bar on fine grain film, then analyze the resulting image to obtain the point spread function. Even the exposure of a general, but known, object might lead to a knowledge of the system since Equation (4) can be rewritten

$$h(x,y) = \mathcal{F}^{-1} \quad \frac{G_1(u,v)}{F(u,v)} \qquad (7)$$

If the object f(x,y) is known, the distorted image $g_1(x,y)$ is recorded, and the two are registered with respect to each other, then Equation (7) might be used to obtain the system PSF.

Laboratory tests of the S-056 telescope imaging characteristics were made prior to the start of the work reported here. Since these tests were not intended for PSF estimation their usefulness is uncertain. Although distorted images of point sources were made during the test, only visible light and X-ray images of the Air Force resolution chart (shown earlier) have been made available to date. The software necessary for analyzing the distorted images and for applying Equation (7) has been developed and some preliminary work has been done toward applying Equation (7) to computer generated data. Because of the requirement to register the images $g_1(x,y)$ and f(x,y) relative to each other, this technique has not been attempted on real data.

(b) If a reasonable model for an imaging system can be developed then a theoretical analysis may be used to predict its point spread function. Since Wolter's (5) model and resulting equations were used to design the S-056 X-ray telescope, they seem to be a logical choice to use for predicting the S-056 system point spread

function. These equations do not include factors for describing abnormalities arising during construction (such as deviations from the true paraboloid-hyperboloid curve, surface roughness, etc.), therefore they will not lead to an exact prediction of the system PSF. They do, however, provide a good initial estimate. A ray tracing procedure based on Woltor's equations was used to assess the imaging properties of the S-506 telescope. This analysis was performed by Sperry Rand Corporation (6). The simulation produced a set of PSF's for various off-axis locations. Two of the important conclusions drawn from the Sperry study were: (1) the PSF is shift-varient (i.e., the shape of the PSF is not constant over the field of view) and, (2) the PSF is not circularly symmetric. The system PSF is shift-invarient over a limited field of view, however, and the deviation from circular symmetry is slight for on-axis images. Therefore, for purposes of simplicity the PSF was assumed to be shift-invarient and circularly symmetric. Since all the images received to date were photographed on-axis, this is not a bad preliminary assumption. The "circularly symmetric" on axis, system point spread function which was predicted by ray-trace analysis of the S-056 telescope is shown in Figure 27.

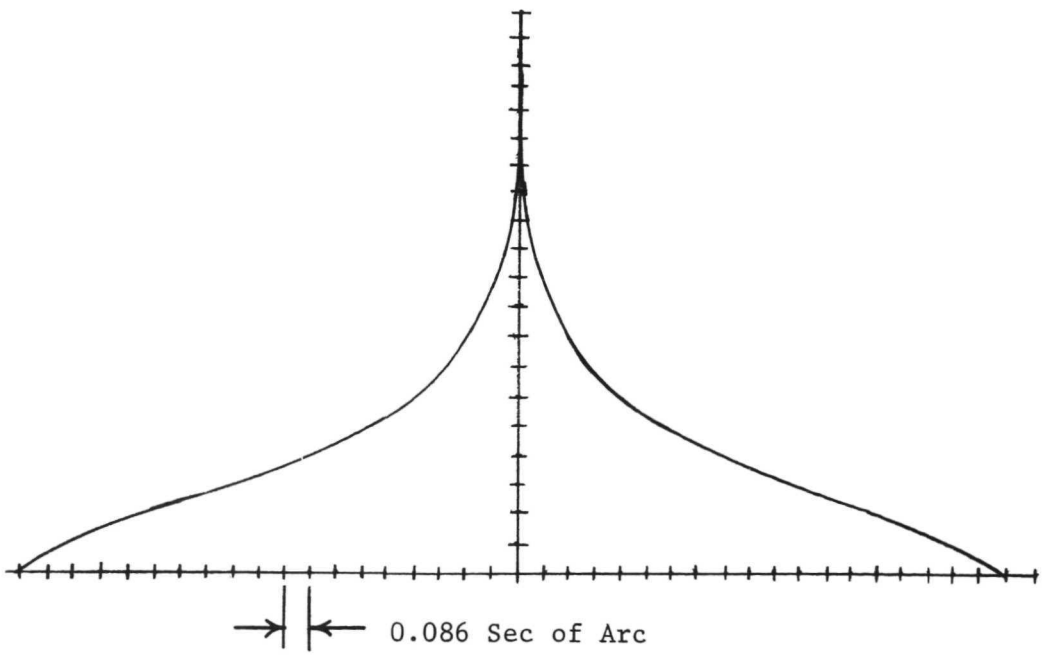


Figure 27 - Thecretical Prediction of S-056 PSF for On-Axis Images at Infinity

(c) If the original scenes of the flight images of the S-056 telescope contain any sharp points or sharp edges, then it may be possible to perform an analysis of flight images to determine the system point spread function. Such an analysis of the iamge of a single sharp point is straight forward but when applied to more complex patterns, the technique becomes much more involved. Specifically, if the degrading system is circularly symmetric then only one sharp edge is required. If however, it is not circularly symmetric then sharp edges running in many directions are required. Therefore, if any single sharp edge is to be used to estimate the system PSF, it should be imaged on-axis. One major obstacle in this method of estimating the system point spread function is the film grain noise in the degraded image. Suitable point images (with respect to the resolution of the telescope) may appear on the sun during the flight of the S-056 telescope, and if the flight schedule remains as planned, a solar eclipse will also provide an image of a sharp edge which is suitable for analysis.

An immediate question arises when one considers the problems of image deconvolution. That is, "How accurate must the PSF estimate be in order to improve a distorted image?" In an effort to answer this question, the following study was performed.

A resolution chart was generated using the IDAPS RESOLUTION CHART operator as shown in Figure 28. Since this test image was computer generated, it was free of film and scanner noise. The test image was then convolved with the PSF predicted for the S-056 telescope using IDAPS operator FORCON. The resulting blured image (see Figure 29) is a fair example of the kind of distortion that could be expected from S-056 if all the noise and nonlinear aberration could be eliminated (this is the function $g_1(x,y)$ in Figure 17). Starting with the predicted S-056 PSF, an array of various PSF profiles was constructed (see Figure 30) with the predicted PSF in the center. In this array, the PSF base width increases from left to right and the average slope of their sides increases from top to bottom. In each case the PSF is normalized.

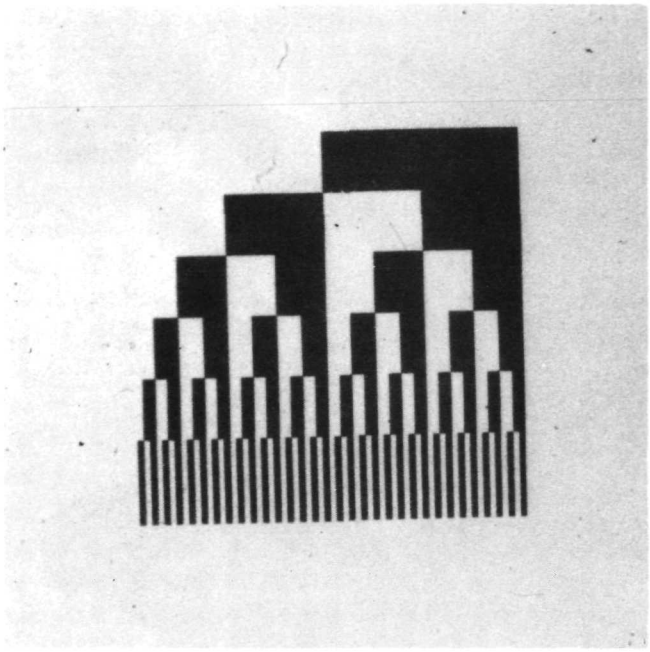


Figure 28 - Computer Generated Resolution Chart Used in Testing the Dependency of Deconvolution on Accurate PSF Determination

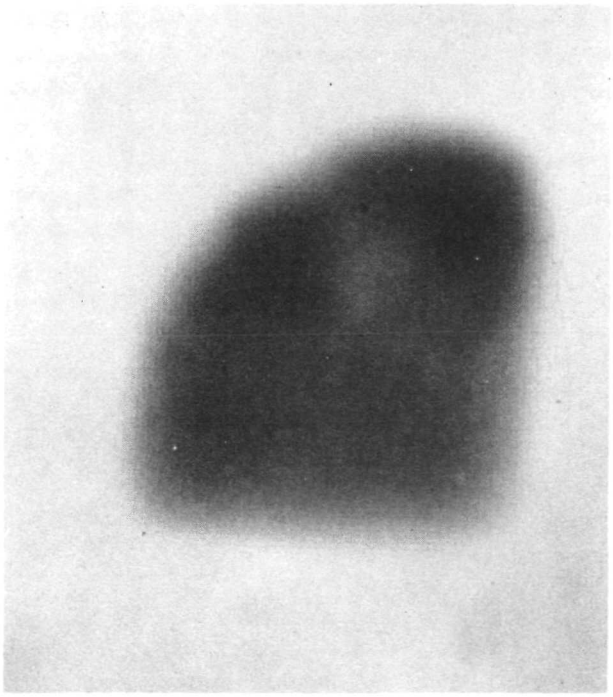


Figure 29 - Computer Generated Resolution Chart Blurred By Convolution with Predicted S-056 PSF

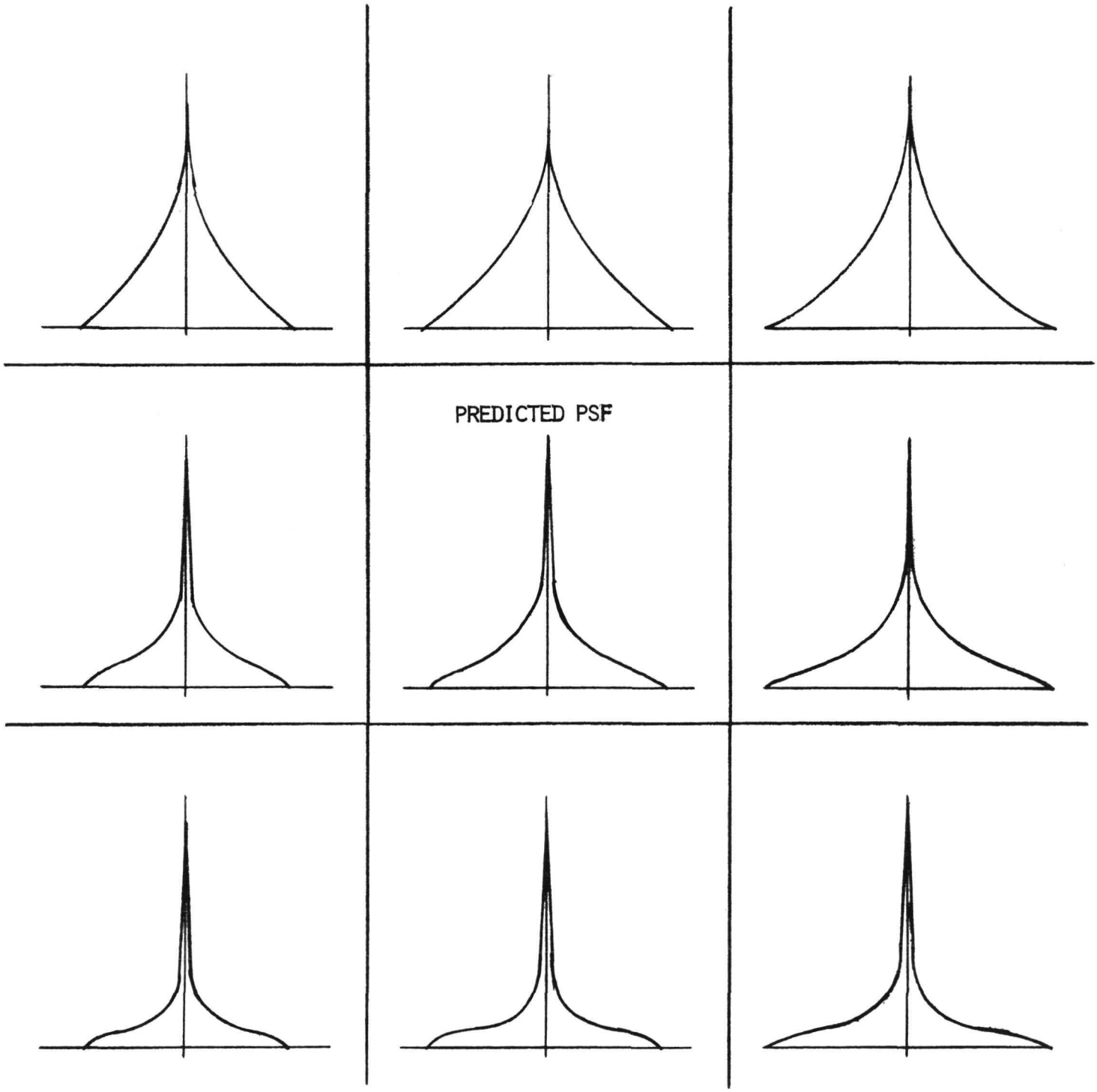


Figure 30 - 3 x 3 Array of Variations on Predicted S-056 PSF (Predicted Curve is in the Center)

The blurred resolution chart of Figure 29 was deconvolved (direct implementation of Equation (4)) with each of the PSF's and the results of the deconvolutions are shown in Figure 31.

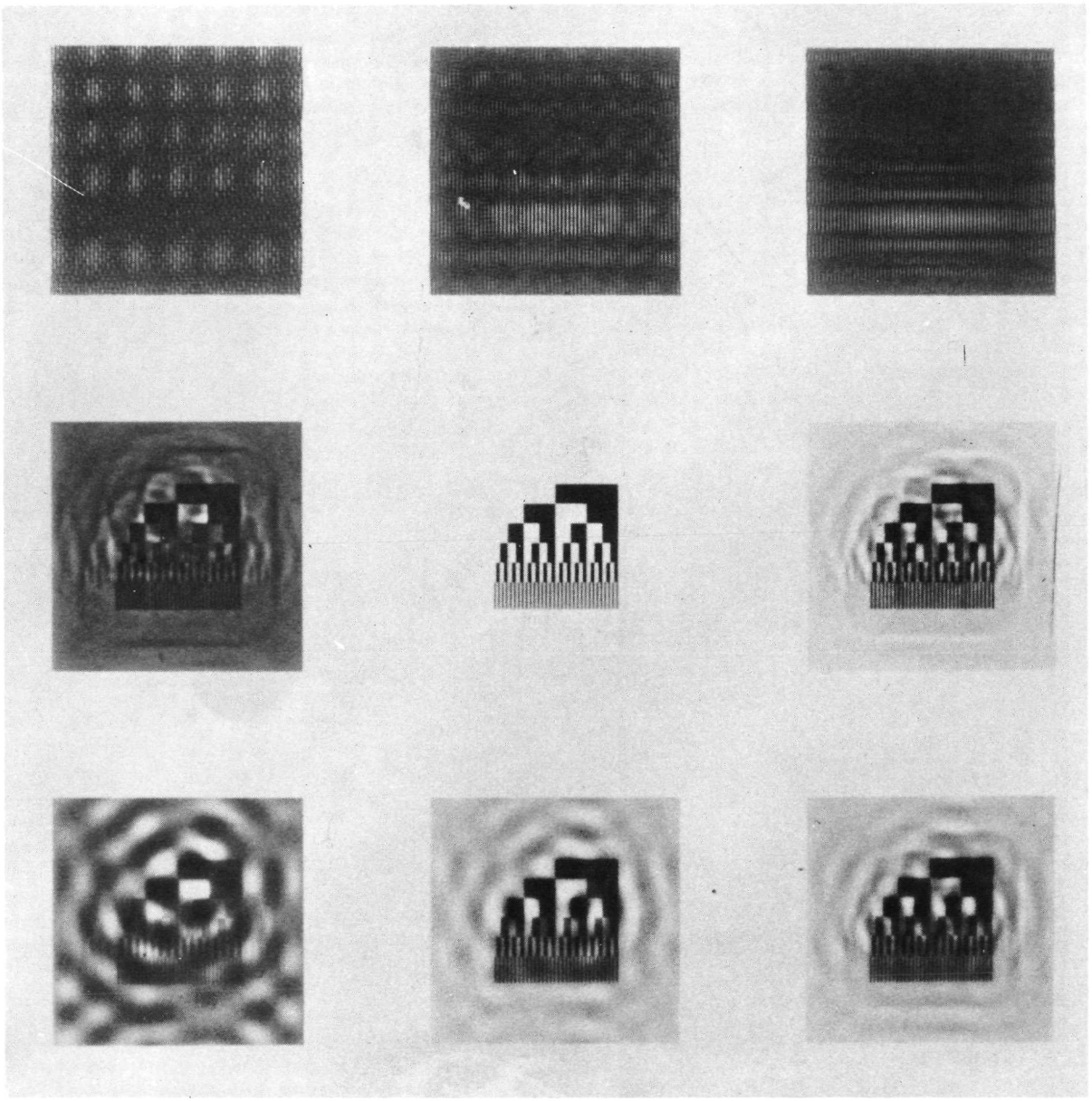


Figure 31 - Results of the Deconvolution of the Blurred Image in Figure 29 With Each of the PSF's in Figure 30

Each deconvolved image corresponds to the PSF occupying the respective position in Figure 30. An analysis of the deconvolved images reveals several important facts: (1) the center image (the one deconvolved with the true system PSF) is indeed restored exactly to its original form, (2) the images of the first row are all dominated by frequency correlated noise to the extent that no image is visible, (3) the resolution charts in the images on the second row are all brought into sharp focus -- the blurring seems to be under corrected in the first image and over corrected in the last -- both exhibit a "ringing" noise, and (4) the resolution charts in the images in the third row are not brought into sharp focus -- but they have still been improved through deconvolution. The "ringing" present in several of the images is due to an overamplification of certain frequency terms. This is the same thing which caused the correlated noise in the images of row one except in the case of the "ringing" the overamplification was not strong enough to completely dominate the picture.

The preceeding study led to an understanding of the PSF estimation accuracy required for successful deconvolution. It appears, however, that absolute accuracy in PSF estimation is not essential and significant improvement can be obtained by applying inexact PSF's in the process.

3.3. APPLICATION TO REAL DATA

One of the photographs of the modified Air Force resolution chart, taken during the "face-to-face" testing of the S-056 telescope, served as subject image for most of the real data investigations of this project. A photomicrograph of this image which was designated Visible Light Frame 9, was presented in Figure 7 of Section 1. The image of Frame 9 was scanned with a microdensitometer and converted to digital format for computer processing. The scan data was reproduced on photographic film and an enlargement of this image is presented in Figure 32. No computer processing was performed on this image. Losses and noise attributable to the scanning process may be observed (compare Figure 32 to Figure 7). The scanning of the Visible Light Frame 9 resulted in an 80 element x 80 element array of quantization values ranging from a minimum gray value of 4 to a maximum of 52.

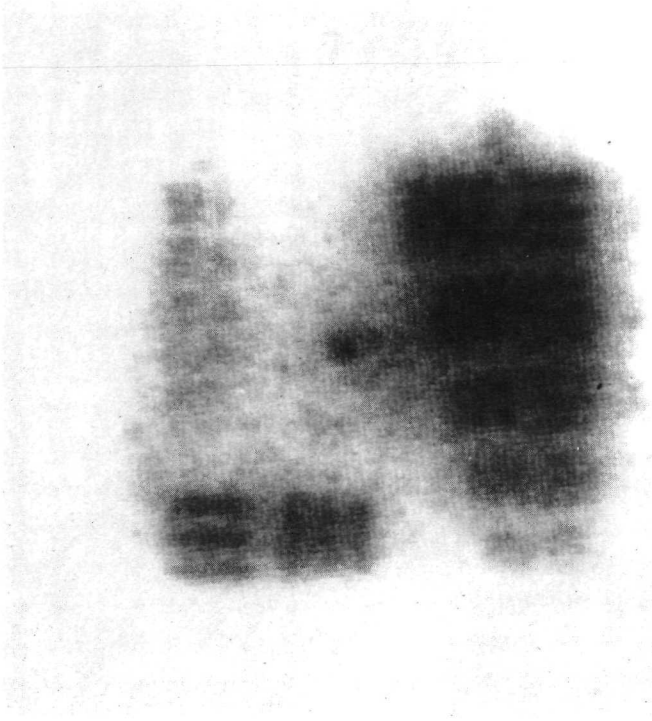


Figure 32 - Visible Light Frame 9 After Scanning with a Microdensitometer and Re-recording on Film

3.3.1 PSF Estimation

One of the first problems addressed in the study of real S-056 data was the problem of finding a point spread function which would produce significant improvement when used to deconvolve the real data.

At first the ray trace prediction PSF was used to deconvolve the Visible Light Frame 9. The result of this effort was an image which was somewhat less blurred, but which was very noisy. Since deconvolution with the predicted PSF did not result in a suitable improvement of the distorted image, an iterative procedure was initiated. First, several new PSF's were generated by varying the predicted PSF's: (a) base width, (b) rate of slope, and (c) shape. The resulting PSF's varied considerably from the predicted PSF. Each of the new PSF's was then used to deconvolve the test image. A new set of PSF's were designed by making slight variations in the PSF which produced the best results in the

previous run and the deconvolution series was repeated. This process was continued until variation in the PSF produced little noticeable change in the deconvolved image. Figure 33 contains the images resulting from deconvolution with a typical group of PSF's.

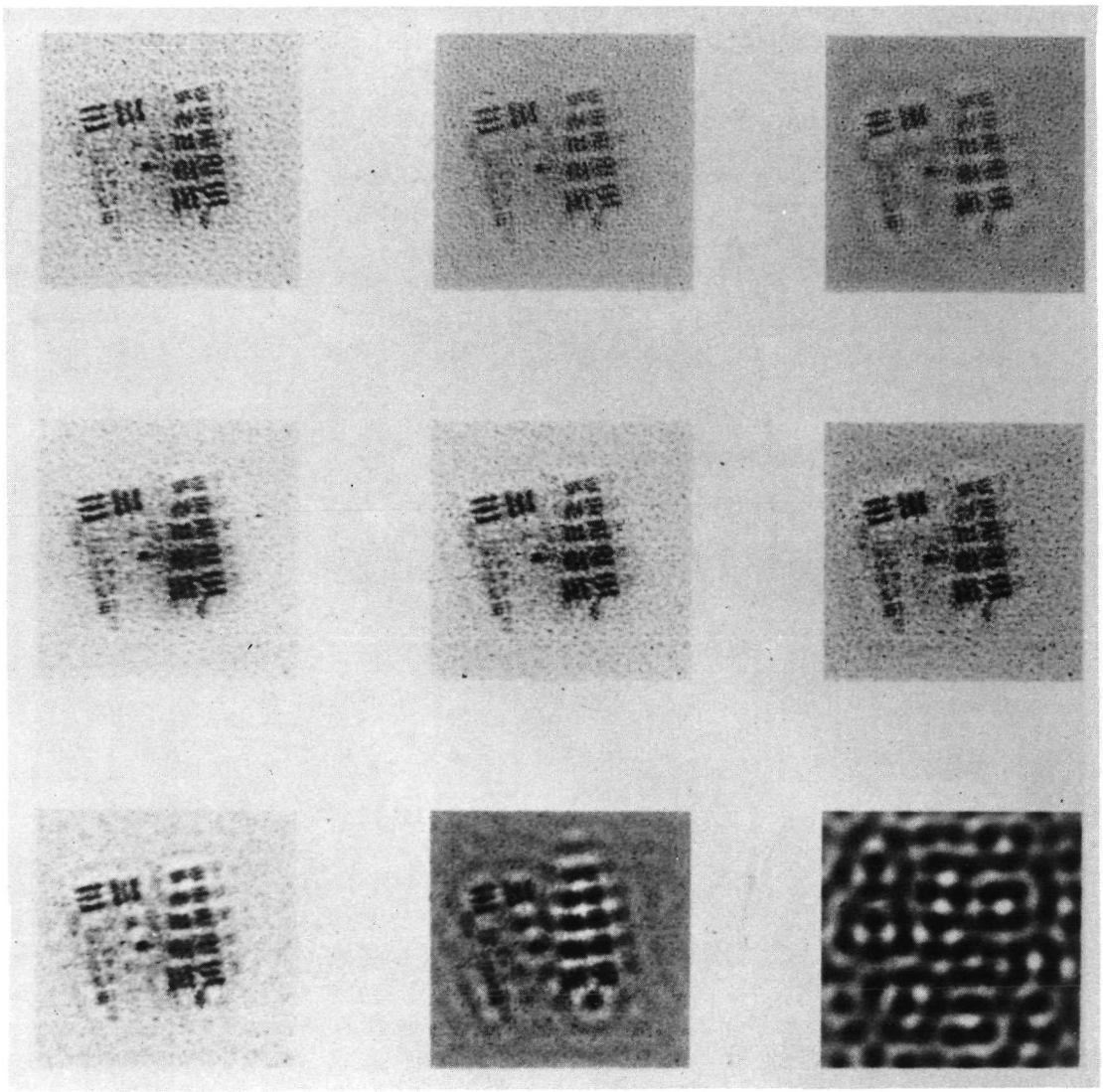


Figure 33 - Results of the Deconvolution of Visible Light Frame 9 With an Array of Trial PSF's

The center image was selected as the one having the greatest overall improvement. Figure 34 compares the point spread function which generated this image (curve (a)) with the one predicted by ray trace analysis (curve (b)).

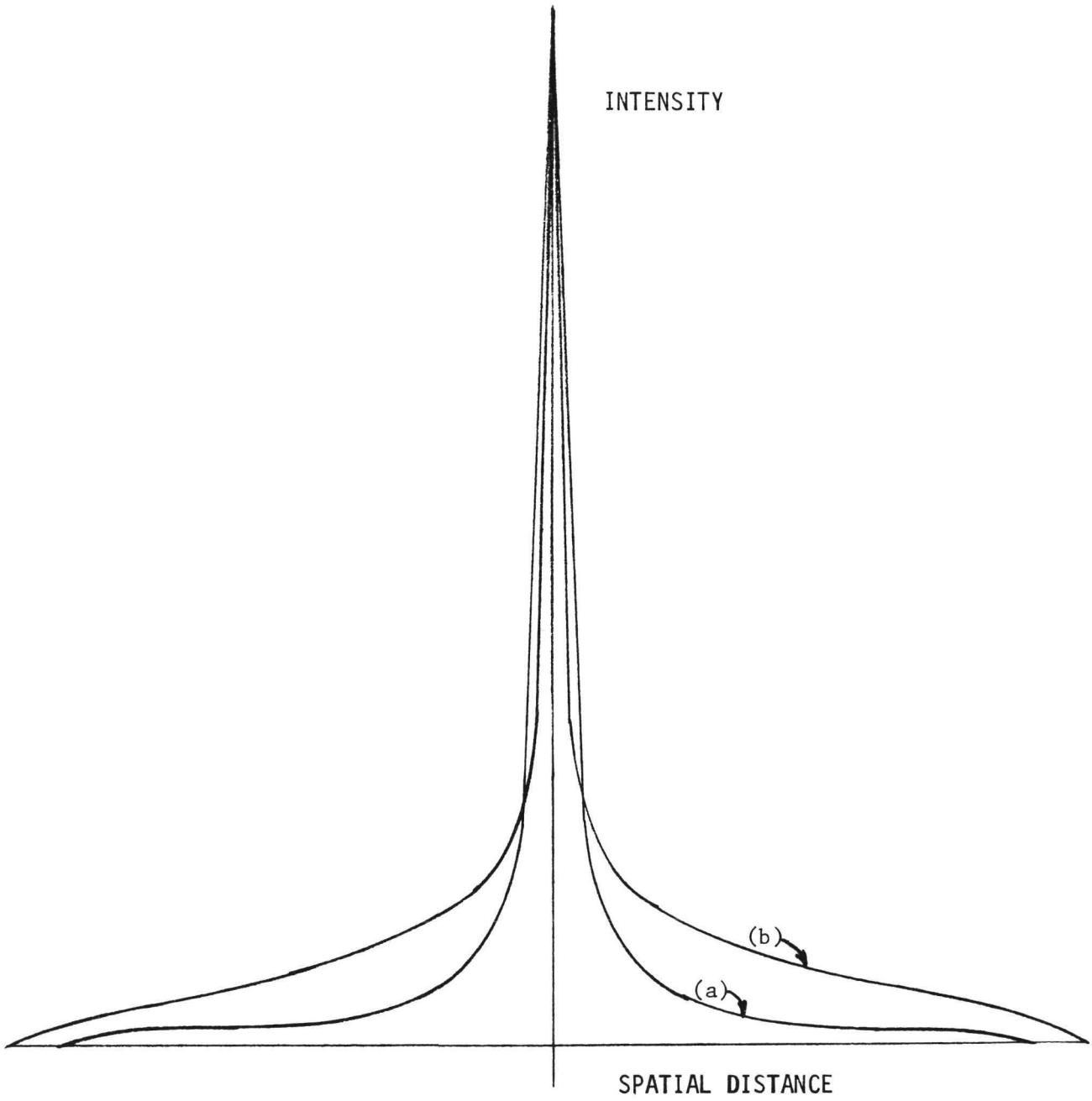


Figure 34 - Comparison of PSF Producing Best Deconvolution of Visible Light Frame 9 (a) With Ray Trace Predicted PSF (b)

Since the refined curve is closer to a unit impulse than the predicted curve, its Fourier transform will tend to be more uniform than the transform of the predicted PSF (the transform of a two-dimensional unit impulse is a flat surface). Therefore, deconvolution with PSF curve (a) will tend to produce a more uniform amplification of frequency terms than curve (b). This simply indicates that correction must sometimes be reduced in order to keep the noise level down in deconvolved images. The center subframe of Figure 33 which was produced by straight forward deconvolution with no controls, shows considerable reduction in blur and improved contrast.

3.3.2 Deconvolution Controls

The direct application of Equation (4) will not yield the best results obtainable through deconvolution due to the presence of noise and non-reversible system nonlinearities. Three methods of direct control of the deconvolution process are applicable to S-056 photographs:

- Scaling
- Frequency Selection Processing
- Amplification Limiting

3.3.2.1 Scaling - When an image is blurred, it looses some of its contrast. That is, the difference between the lightest and darkest parts of the image becomes less and less. The ultimate blurring of an image is reached when all detail in the image fuses into a single neutral gray level. Deconvolution enhances the contrast in an image. Images resulting from deconvolution of a noise free image with a true system point spread function will thus have a gray scale range greater than the input image. In the presence of noise, the range of the deconvolution output may exceed the range acceptable as input to the available photo recording and display equipment (64 levels). In such cases, the output image must be rescaled to 64 levels or less.

In cases of severe noise domination, it may be desirable to limit the upper and lower gray levels between which data is scaled. Generally, the effects of low-level noise may be reduced by setting the lower level for scaling at or near the level of the low-level noise. Thus, the noise below this limit is not considered in the output picture. Also, by setting a maximum limit for scaling at the peak level of the valid data, high amplitude noise spikes are "clipped" which might otherwise, because of the scaling process, dominate the valid data.

The center image of Figure 33 was chosen as the best deconvolved real data image resulting from the system point spread function search. The images in Figure 33 as well as all the other pictures used in the PSF search were scaled between their maximum and minimum values. If the images had been scaled between a narrower set of high/low clipping limits, some of the background noise could have been reduced and contrast improved. Figure 35 illustrates the result of using various high/low clipping limits for scaling the center image of Figure 33. Figure 36 is a compilation of the upper and lower clipping levels beginning with the upper left image and continuing left to right, top to bottom. The center image of Figure 35 exhibits the best overall improvement with respect to contrast, definition, noise level, etc.

In general, the optimum clipping levels will have to be determined for each class of images processed. Multiple display comparisons, such as presented in Figure 36 are prepared by the IDAPS operator MULTIPLE DISPLAY and are useful in evaluating a number of trial runs in order to determine which run conditions yield the best image.

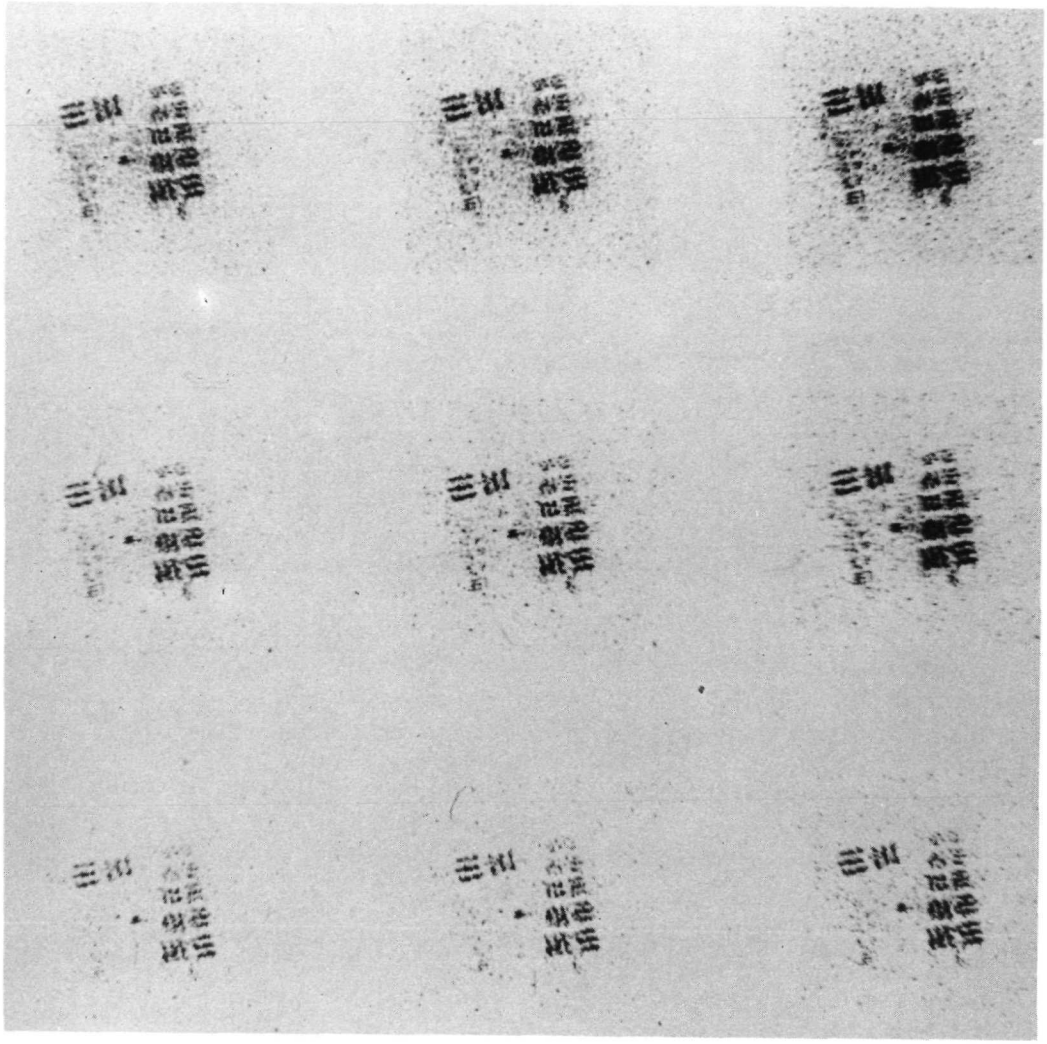


Figure 35 - Results of Scaling the Data From the Deconvolution of Visible Light Frame 9 Between the High/Low Limits in Figure 36

IMAGE	UPPER CLIPPING LEVEL	LOWER CLIPPING LEVEL
1	123	0
2	93	0
3	63	0
4	123	20
5	93	20
6	63	20
7	123	40
8	93	40
9	63	40

Figure 36 - Image Clipping Levels

3.3.2.2 Frequency Selection Processing - Typically, the deconvolution process consists of amplifying intermediate-to-high spatial frequency components to bring them back to their original level in the original scene. An imaging system will usually attenuate mid-to-high spatial frequencies more than the low ones. Therefore, the higher frequencies will become more susceptible to noise. Substantial improvement may be seen in images which are deconvolved with the system point spread function only over the low-to-intermediate frequency range. This type of deconvolution often improves the distorted image without increasing the visible noise in the image. The frequency at which amplification should be reduced depends upon the noise in the input image and thus can be best determined by an iterative process.

Using the best estimate PSF and the scaling procedure of the previous section, the S-056 visible light image was deconvolved over various pass bands. In each case, normal amplication was allowed on all frequencies below a variable cutoff and an amplification of one was allowed for frequencies above the cutoff. The transition in amplification was gradual.

Figure 37 illustrates the controlled deconvolution process for nine different cutoff frequencies. The upper left image resulted from deconvolution with a high cutoff frequency. The cutoff frequency was decreased from left to right, row by row, until it reaches its lowest value in the lower right image. A careful analysis of the images indicates that background noise may be reduced significantly by frequency selective deconvolution but that care must be taken in selecting the frequencies processed since too much control will blur the image. The center image exhibits the best overall improvement in this series.

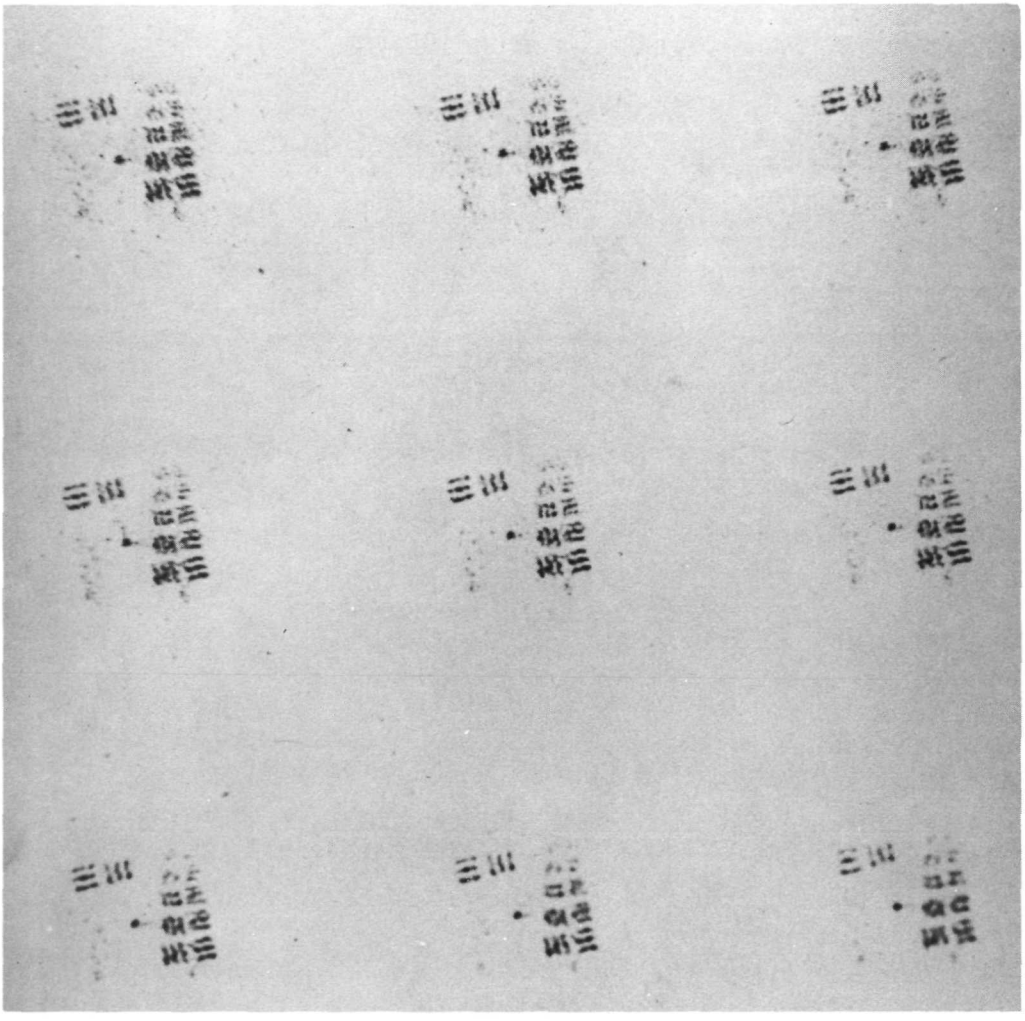


Figure 37 - Results of Frequency Selection Processing of Center Picture in Figure 35

3.3.2.3 Amplification Limiting - For more complex system point spread functions the suppression of frequency terms may not occur only at high frequencies but may be scattered throughout the frequency range. In the absence of noise, and for a true system PSF, small values of H(u,v) (refer to Equation (4)) will be offset with corresponding values of $G_1(u,v)$ so that each $G_1(u,v)$ term will be amplified exactly the amount required to restore the picture. Noise or an incorrect choice of system PSF may, however, prevent the cancellation, thus very

large frequency amplifications may result. The simplest control for such over-amplification of frequencies is to limit the amplification of all frequency terms to some maximum value. In this approach, Equation (4) is restricted to read,

$$f(x,y) = \mathcal{F}^{-1}\left[\frac{G_1(u,v)}{H(u,v)}\right] \qquad |H(u,v)| \leq R \qquad (8)$$

Consider the image shown in Figure 38. (Figure 38 is a reproduction of the noise dominated picture in the center of the first row of Figure 31). This image has been destroyed during deconvolution by a gross misamplification of a few frequency terms.

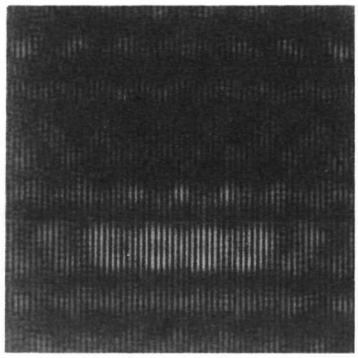
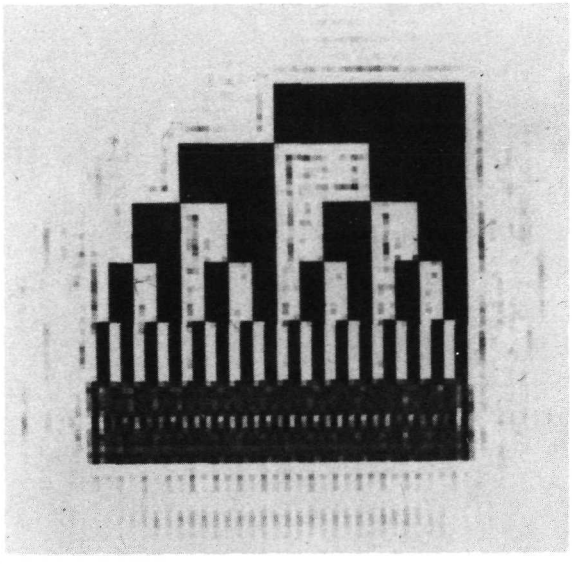
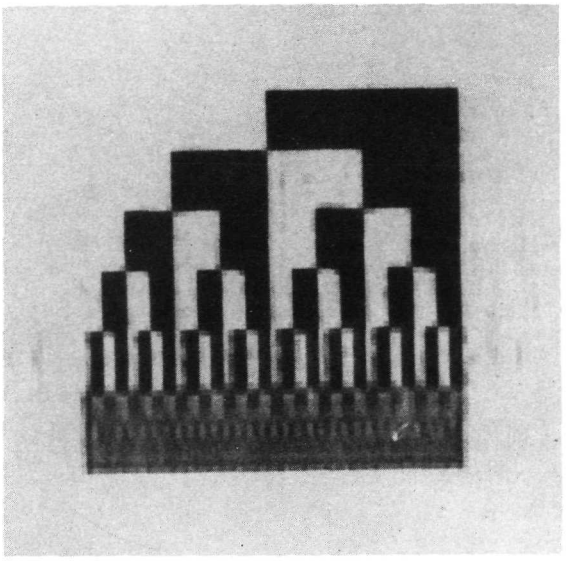


Figure 38 - Deconvolved Resolution Chart with Overamplification of Certain Frequence Terms

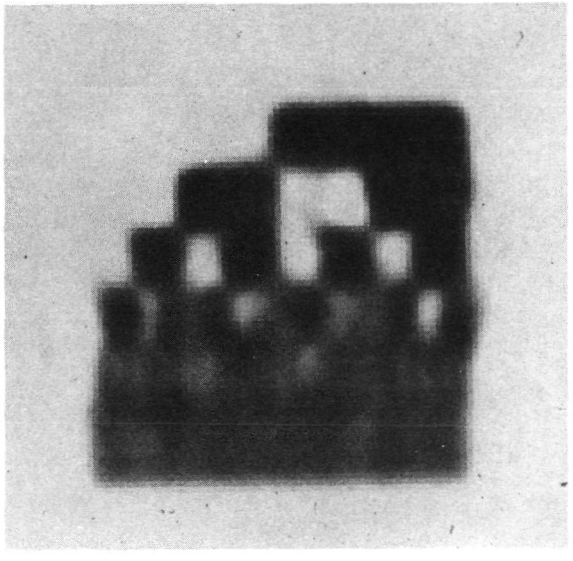
By limiting R to values of one million, 30 thousand and one thousand, the resolution chart is recovered to the extent shown in Figure 39(a), (b), and (c), respectively. All of these images show considerable improvement. The higher frequencies of the original image are not restored because the PSF used in the deconvolution of the image did not pass these frequencies. If the limit is too severe, little or no correction of the blurred image will result.



(a)



(b)



(c)

Figure 39 - Results of Repeating the Deconvolution Illustrated in Figure 38 with Frequency Term Amplification Limited to: (a) 100,000; (b) 30,000; (c) 1,000

Additional studies have indicated that the optimum value of R depends upon the input image and the estimated PSF. It will probably have to be determined through an iterative process. There have been no investigations made on the effect of phase limiting, however, IDAPS does have the provision for limiting both magnitude and phase amplification.

SECTION 4. CONCLUSIONS AND RECOMMENDATIONS

During the past year, the System Development Corporation task team has studied the use of deconvolution techniques for restoring image data from the S-056 experiment as well as such associated techniques of image restoration, enhancement and analysis as are needed to support deconvolution. The efforts of the past year have given considerable insight not only into the problems of S-056 image deconvolution but into many of the more general image data processing requirements of the experiment as well. In fact, the most important product of this effort is not the preliminary techniques for image restoration described in this volume or the software design contained in Volume II, but rather is the general understanding of the total technical requirements for image data processing of the experiment and of the problems that must be solved if a satisfactory image processing capability is to be developed.

4.1 CONCLUSIONS

It is impossible to sum up all that has been learned during the past year, but a few of the more important findings deserve some special attention.

First, the efforts of the past year prove that the restoration and enhancement of S-056 image data by digital techniques are possible and that through the proper application of such techniques, far more valuable scientific data may be recovered from experiment photographs than would be possible otherwise.

Secondly, the extent to which S-056 images may be restored depends heavily on a number of factors:

- The level of noise that accompanies the image data;
- The accuracy with which the image data recorded on film is described to the computer as well as the accuracy of the description of the conditions under which the image data was obtained; and,

- The responsiveness of the system to user needs in carrying out desired techniques of image restoration.

Finally, in addition to the areas of image restoration and enhancement addressed by this project, work is needed to develop techniques for presenting the image data for visual analysis and for assisting in the analysis of the data both by visual means and otherwise.

4.2 RECOMMENDATIONS

From the conclusions outlined above, recommendations for continuing the development of image data processes to support the S-056 experiment include:

- More work is needed to develop the deconvolution technique for S-056 applications. Deconvolution of additional test images should be attempted and more efficient and accurate methods for determing point spread functions for use in deconvolution are needed. A better understanding is needed of the influence of scanning accuracies, noise, nonlinearities, etc. on the deconvolution process.

- Much more efficient methods for dealing with noise must be found. Ways to accurately register multiple frames for multiframe averaging should be developed. Applicable noise removal techniques should be studied with respect to deconvolution to determine their relation to deconvolution -- when they should be applied, under what circumstances, and in what order.

- The accuracy with which image data is extracted from photographic film should be improved. Scanning and quantizing resolution should be improved to provide a scanning accuracy of no less than two microns and a quantizing accuracy of at least 256 levels.

- Linearization data must be obtained as well as any other pertinent information about the S-056 flight film or the equipment used in converting the image data to computer format. Accurate film characteristic curves should be determined for S-056 flight film in all of the regions of the electromagnetic spectrum in which it will operate. Characteristic curves for film scanning equipment are also needed in order to accurately account for scanner non-linearities and noise.

- A simple, direct means of control and feedback is needed to provide the scientist/user of the image processing system with the kind of responsiveness that will be necessary for the handling of the volume of data expected from S-056. An interactive system is needed which provides a means for selecting frames of data, portions of a frame, or specific information for processing and which allow the user to apply available image processes to the data and retrieve his output with a minimum of special instruction.

- Efforts should be directed to the development of techniques for image data analysis such as area, velocity, flux density, and rate of growth calculations, and of techniques for image data presentation such as time lapse cinematography, pseudo-color presentation, iso-intensity plots and stereographic presentations.

- Additional computer software should be developed to support all of the above efforts. Additional software is particularly needed to carry out more advanced forms of digital filtering and to perform the geometric manipulations needed to complement the image registration mentioned above.

REFERENCES

(1) Wilder, W. C., "Properties of the Human Visual System as an Image Evaluator", Department of Electronic Engineering, Purdue University, 1971.

(2) McGlamery, B. L., "Image Restoration Techniques Applied to Astronomical Photography", Astronomical Use of Television - Type Image Sensors - Symposium at Princeton University, 1970.

(3) Harris, James L., "Image Evaluation and Restoration", Journal of the Optical Society of America, Vol. 56, No. 5, May 1966.

(4) Huang, T. S., Schreiber, W. F., Tretiak, O. J., "Image Processing", Proceedings of the IEEE, Vol. 59, No. 11, November 1971.

(5) Wolter, H., "Spiegelsysteme Streifenden Einfalls als Abbildende Optiken für Röntgenstrahlen", Annalen der Physik 10, 94, 1952.

(6) "Analytical Study of the Imaging Characteristics of the Goddard ATM X-ray Telescope", SP-505-0279, Sperry Rand Corporation, 1969.

(7) Blackman, R. B., and Tukey, D. W., The Measurement of Power Spectra, New York: Dover, 1958.

(8) Andrews, H. C., Pratt, W. K., Caspari, K., Computer Techniques in Image Processing, New York: Academic Press, 1970.

(9) Cooley, J. W., and Tukey, J. W., "An Algorithm for the Machine Calculation of Complex Fourier Series", Math. Comput., Vol. 19, pp. 297-301, April 1965.

(10) Bergland, G. D., "The Fast Fourier Transform Recursive Equations for Arbitrary Length Records", Math Comp., Vol. 21, 1967.

BIBLIOGRAPHY

"Analytical Study of the Imaging Characteristics of the Goddard ATM X-ray Telescope" SP-505-0279, Sperry Rand Corporation, 1969.

Andrews, H.C., Pratt, W.K., Caspari, K., Computer Techniques in Image Processing, New York: Academic Press, 1970.

"Apollo Applications Program (AAP) Payload Integration: S-056 Quartz Mirror Test", NASA Contract NAS8-24000, Martin Marietta, 1970.

Bergland, G.D., "A Guided Tour of the Fast Fourier Transform", IEEE Spectrum, July 1969.

Bergland, G.D., "The Fast Fourier Transform Recursive Equations for Arbitrary Length Records", Math Comp., Vol. 21, 1967.

Billingsley, F.C., "Applications of Digital Image Processing", Appl. Opt. Vol. 9, February 1970.

Billingsley, F.C., "Noise Considerations in System Design", Unpublished paper given at Short Course on Image Processing, Purdue University, June 1971.

Blackman, E.S., "Effects of Noise on the Determination of Photographic System Modulation Transfer Function", Photogr. Sci. Eng., Vol 12, Sept. - Oct. 1968.

Blackman, E.S., "Recovery of System Transfer Functions from Noisy Photographic Records", Proc. SPIE Seminar on Image Information Recovery, Philadelphia, Pa. 1969.

Blackman, R.B., and Tukey, D.W., The Measurement of Power Spectra, New York: Dover, 1958.

Boyce, B.M., "The Role of Image Processing in Synthetic Aperture Systems and Aberrated Axially Symmetric Systems", Proceeding of Symposium on Sampled Images, Perkin-Elmer Corp., 1971

Brigham, E.O., and Morrow, R.E., "The Fast Fourier Transform", IEEE Spectrum, Vol. 4, Dec. 1967.

Cooley, J.W., and Tukey, J.W., "An Algorithm for the Machine Calculation of Complex Fourier Series", Math Comput., Vol. 19, April 1965.

Danielson, R.E., and Tomasko, M.G., "Image Processing of Stratoscope Photographs", NASA SP-256, May 1970.

Experiment Requirements Document for X-Ray Telescope (Experiment S-056). Huntsville: George C. Marshall Space Flight Center, April 22, 1970.

Fellgett, P., "Concerning Photographic Grain Signal-to-Noise Ratio, and Information", Journal of the Optical Society of America, Vol. 43, No. 4, April 1953.

Garriott, O.K., Forsythe, D.L., Cagle, E.H., "Instruments, Systems, and Manned Operations of the Apollo Telesceope Mount", Astronautics and Aeronautics, June 1971.

Gentleman, W.M., and Sande, G., "Fast Fourier Transforms - For Fun and Profit", 1966 Fall Joint Computer Conf., AFIPS Proc., Vol 29, Washington, D.C.: Spartan Books, 1966.

Harris, J.L., "Diffraction and Resolving Power", Journal of the Optical Society of America 54, No. 7, July 1964.

Harris, J.L., "Image Evaluation and Restoration", Journal of the Optical Society of America 56, No. 5, May 1966.

Harris, J.L., "Potential and Limitations of Techniques for Processing Linear Motion-Degraded Imagery", Journal of the Optical Society of America, 56, No. 5, May 1966.

Harris, J.L. "Restoration of Atmospherically Distorted Images", Scripps Inst. Oceanography, Univ. California, San Diego, SIO Ref. 63-10, March 1963.

Hawkins, J.K. and Munsey, C.J., "Image Processing by Electro-Optical Techniques", Journal of the Optical Society of America, Vol. 57, No. 7, July 1967.

Helstrom, C.W., "Image Restoration by the Method of Least Squares", J. Opt. Soc. Amer., Vol. 57, March 1967.

Huang, T.S., Schreiber, W.F., Tretiak, O.J., "Image Processing", Proceedings of the IEEE, Vol. 59, No. 11, November 1971.

Lipkin, B.S., Rosenfeld, A., Picture Processing and Psychopictorics, New York: Academic Press, 1970.

Mangus, J.D., and Underwood, J.H., "Optical Design of a Glancing Incidence X-ray Telescope", Applied Optics, Vol. 8, No. 1, January 1969.

McGlamery, B.L., "Image Restoration Techniques Applied to Astronomical Photography", Astronomical Use of Television - Type Image Sensors - Symposium at Princeton University, 1970.

McGlamery, B.L., "Restoration of Turbulence-Degraded Images", Journal of the Optical Society of America 57, No. 3, March 1967.

Mueller, P.F. and Reynolds, G.O., "Image Restoration by Removal of Random Media Degradations", Journal of the Optical Society of America, Vol. 57, No. 11, November 1967.

Nathan, Robert, "Digital Video-Data Handling", (Technical Report No. 32-877) Pasadena, California: Jet Propulsion Laboratory, California Institute of Technology, January 5, 1966.

Oppenheim, A.V., Schafer, R.W., and Stockham, T.G., Jr., "Nonlinear Filtering of Multipled and Convolved Signals", Proc. IEEE, Vol. 56, August 1968. (Reprinted in IEEE Trans. Audio and Electroacoustics, Vol. AU-16, Sept. 1968)

Papoulis, A., The Fourier Integral and Its Applications, New York: McGraw-Hill, 1962.

Rosenfeld, Azriel, Picture Processing by Computer, New York: Academic Press, 1969.

Rushforth, C.K., and Harris, R.W., "Restoration, Resolution, and Noise", Journal of the Optical Society of America 58, No. 4, April 1968.

Sellner, H.R., "Transfer Function Compensation of Sampled Imagery", Proceeding of A Symposium on Sampled Images, Perkin-Elmer Corp., 1971.

Slepian, David, "Linear Least-Squares Filtering of Distorted Images", Journal of the Optical Society of America 57, No. 7, July 1967.

Slepian, D., "Restoration of Photographs Blurred by Image Motion", Bell Syst. Tech. J., Vol. 46 December 1967.

Stockham, T.G., "High Speed Convolution and Correlation", 1966 Spring Joint Computer Conf. AFIPS Proc. Vol. 28, Washington D.C.: Spartan, 1966.

Wilder, W.C., "Properties of the Human Visual System as an Image Evaluator", Dept. of Elec. Eng., Purdue University, 1971.

Wolter, H., "Spiegelsysteme Streifenden Einfalls als Abbildende Optiken für Röntgenstrahlen", Annalen der Physik 10, 94, 1952.

APPENDIX A

FOURIER TRANSFORM TECHNIQUES

A.1 CONTINUOUS FOURIER TRANSFORM

The one-dimensional Fourier transform pair for continuous signals can be written as

$$F(f) = \int_{-\infty}^{\infty} f(t)\, e^{-i2\pi ft}\, dt \qquad -\infty < t < \infty$$

$$f(t) = \int_{-\infty}^{\infty} F(f)\, e^{i2\pi ft}\, dt \qquad -\infty < f < \infty \qquad (1)$$

where $i = \sqrt{-1}$, F(f) represents the frequence domain function and f(t) is the time domain function.

If a signal is to be processed on a digital computer then the finite discrete version of the Fourier transform must be employed.

A.2 DISCRETE FOURIER TRANSFORM

If a real valued function f(t) is sampled ever Δt units (seconds, mm, feet) as shown in the Figure A.1,

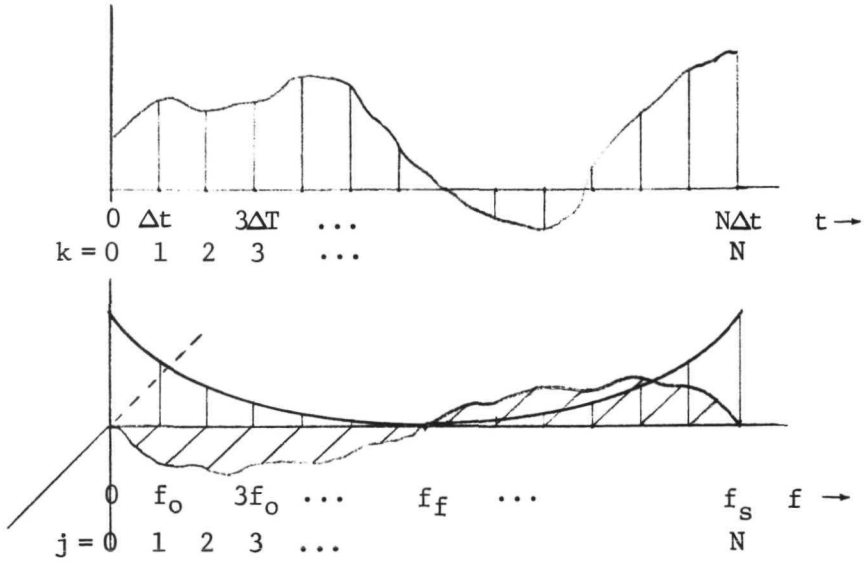


Figure A.1 - Waveform Sampling

the discrete one-dimensional Fourier transform pair would appear as

$$F(j) = \sum_{k=0}^{N-1} f(k)e^{-(i2\pi jk)/N}$$

$$f(k) = \frac{1}{N} \sum_{j=0}^{N-1} F(j)e^{(i2\pi jk)/N} \qquad \begin{matrix} j = 0,1,\ldots,N-1 \\ k = 0,1,\ldots,N-1 \end{matrix} \qquad (2)$$

where (1) $f(k) = f(k\Delta t)$, $F(j) = F(jf_o)$,

(2) the waveform is sampled every Δt units for a period of $T = N\Delta t$, thereby producing a total of N samples,

(3) the frequency is sampled every $f_o = 1/T$, and

(4) the real part of the transform is symmetric and the imaginary part is antisymmetric about $f_f = 1/2\ \Delta t$.

Blackman and Tukey (7) provide a detailed derivation of the discrete Fourier transform.

The time (spatial) series $f(k\Delta t)$ is assumed to be periodic in the time (spatial) domain of period T units, and the Fourier coefficients $F(jf_o)$ are assumed to be periodic over the sample frequency f_s.

A.3 DISCRETE IMAGE TRANSFORMS

An original image may be represented by an array of intensity components over the image surface obtained by two-dimensional spatial sampling. In this report an image array will be considered to be a square array of N^2 intensity samples described by the function f(x,y) over the image coordinates (x,y).

The two-dimensional discrete Fourier transform pair of an image can be expressed by

$$F(u,v) = \sum_{x=0}^{N-1} \sum_{y=0}^{N-1} f(x,y) \exp\left[-\frac{2\pi i}{N}(ux + vy)\right]$$

$$f(x,y) = \frac{1}{N^2} \sum_{u=0}^{N-1} \sum_{v=0}^{N-1} F(u,v) \exp\left[\frac{2\pi i}{N}(ux + vy)\right] \quad (3)$$

Since the transform kernels are separable and symmetric the two-dimensional transform can be computed as two sequential one-dimensional transforms (8). The terms u and v are called the spatial frequencies of the image and are usually specified in terms of cycles/frame.

A.4 FAST FOURIER TRANSFORM

Computer evaluation of the first equation of pair (2) can be effected very efficiently. For computational purposes the equation can be more easily represented in matrix form as

$$[F(j)] = [W^{jk}]\ [f_o(k)]$$

where $[F(j)]$ and $[f_o(k)]$ are N x 1 column matrices and $[W^{jk}]$ is an N x N matrix with

$$W = e^{-i2\pi/N}$$

By factoring the matrix $[W^{jk}]$ properly into component matrices one is able to reduce the number of complex multiplications and additions required by equation (2) and thus decrease the time required for transformation. The Cooley-Tukey Fast Fourier transform algorithm (9), one of the first operation fast algorithms, factors one N x N matrix into γ -(N x N) matrices (where $\gamma = 2^N$) such that each of the new factored matrices has this special property of reducing the number of complex multiplications and additions required.

The component 2 in the relation $Y = 2^N$ is referred to as the base of the fast Fourier algorithm; that is, the Cooley-Tukey algorithm is a base 2 algorithm. Because of the symmetries of the sine and cosine weighing functions, an algorithm of base 4 (or even 8) is more efficient than a base 2 algorithm (10). The base 4 (base 8) algorithm has the disadvantage of limiting the record size to a power of 4 instead of 2. This restriction can be eliminated by constructing a base 4 + 2 algorithm with which one computes as many cycles in base 4 as possible then finishes the computation with a base 2 algorithm. The FFT routine contained in IDAPS and used in the investigations described in this report was a base 4 + 2 algorithm.

The number of multiplications required to perform a straight two-dimensional Fourier transform is N^4 while the number required by a base 2 algorithm is $4N^2 \log_2 N$.